
UNIVERSITÀ DEGLI STUDI DI PADOVA
DIPARTIMENTO DI INGEGNERIA INDUSTRIALE

TESI DI LAUREA MAGISTRALE IN INGEGNERIA CHIMICA
E DEI PROCESSI INDUSTRIALI

# DEVELOPMENT OF CYCLIC BIOMECHANICAL STIMULATION ON A MICROFLUIDIC CHIP

Relatore: Dott. Nicola Elvassore

Laureanda: LIA PREVEDELLO

Anno Accademico 2011-2012

# Summary

Currently in the biological field an increasing interest on cell response to external physical solicitation is rising since accumulating evidence suggest a significant role of mechanical stimulation in several areas such as the development and maintenance of skeletal muscles, the onset and perpetration of several myofiber diseases, and functional and structural changes in the myocardium. Moreover there's a growing list of signaling pathways that are activated in response to mechanical stress in cardiomycytes and in the skeletal muscle cells.

Despite the efforts made so far, the precise mechanisms by which mechanical stress interacts with, and influences, the cell behavior are yet to be discovered. To this end, and to fully exploit biomechanical stimulations in biological research, there is the need to develop innovative devices that allow real-time analysis of mechanically stressed cell cultures.

In this work a novel microfluidic device for biomechanical stimulation is developed, specifically designed to ensure compatibility with the analysis by laser confocal microscopy. The microfluidic chip produced is composed of three layers: a microscopy glass on which a system of channels is chemically etched, an elastomeric membrane on which cells are plated, and that will endure the actual mechanical deformation, and a microfluidic channel that ensures the delivery of nutrients and, if needed, chemical signals to cultured cells. The design and manufacturing of each layer was analyzed and optimized to maximize the deformation achievable and the culturing conditions. The final device was then tested to check the fluidic-based control of deformation and finally an experiment was performed to verify the mechanical stretch of cultured cells.

# Riassunto

Negli ultimi anni diverse scoperte scientifiche hanno dimostrato l'importanza degli stimoli meccanici nel corretto sviluppo di organi e tessuti, inoltre è stata dimostrata la correlazione tra stress meccanico e molte patologie muscolari e cardiache. Da queste osservazioni è nato il campo della biomeccano-trasduzione, volto a studiare la traduzione cellulare di stimoli meccanici in segnali biochimici, processo che permette alle cellule di adattarsi all'ambiente circostante.

Nello specifico gli sforzi meccanici esterni influiscono sulla miogenesi (il processo di attivazione di cellule primarie in mioblasti, il loro differenziamento in miociti e la loro fusione in miotubi), attivando precocemente le cellule satellite normalmente quiescenti o, successivamente, favorendo la proliferazione dei mioblasti a discapito del loro differenziamento in miociti.

La presenza di sforzi meccanici è anche responsabile di diversi danni muscolari, in particolare indebolendo la membrana cellulare fino a causare microrotture attraverso cui vi è uno scambio non fisiologico di ioni e proteine dall'ambiente esterno verso l'interno della cellula e viceversa. Un campo particolarmente interessante nell'applicazione di deformazioni meccaniche è lo studio della distrofia muscolare di Duchenne, una malattia genetica degenerativa che colpisce circa 1 bambino ogni 3500 e conduce a una morte precoce, generalmente entro i 20 anni.

La biomeccanica è applicata anche allo studio di cardiomiociti, cellule che *in vivo* crescono in uno degli ambienti più attivi dal punto di vista meccanico. Nello specifico, in questo campo si vuole riprodurre un ambiente il più possibile simile alle condizioni *in vivo* per favorire il differenziamento di cellule staminali in cardiomiociti da sfruttare nella terapia con cellule staminali per il recupero della funzionalità cardiaca in seguito a infarto del miocardio.

Tutte queste applicazioni della meccano-trasduzione sono volte a capire più nel dettaglio i complessi meccanismi di differenziamento cellulare e produzione di tessuti o organi e nell'individuare nuovi *target* per terapie volte a curare malattie muscolari o cardiache.

In questo lavoro vengono presentati la progettazione e lo sviluppo di una camera per la coltura cellulare in condizioni di stress meccanico ciclico. Grazie all'impiego delle tecnologie microfluidiche il sistema non solo permette un accurato controllo delle condizioni di coltura, ma risulta essere particolarmente compatto riuscendo così ad essere interfacciato con il microscopio confocale, uno strumento di misura e *imaging* molto usato in campo biologico. Al fine di garantire la possibilità di effettuare analisi in tempo reale al microscopio confocale al massimo ingrandimento disponibile (64x) la distanza del piano focale delle cellule dall'obiettivo non deve superare i 200μm e il piano focale deve rimare fisso durante la deformazione. Inoltre è richiesta la possibilità di deformare le cellule di almeno il 15% rispetto alla lunghezza iniziale.

Il dispositivo ideato a tale scopo si compone di tre strati: un vetrino per microscopia, una membrana elastomerica e un sistema microfluidico realizzato in poli(dimetilsilossano), PDMS. Il vetrino, oltre a fungere da substrato rigido, viene corroso mediante attacco con acido fluoridrico al fine di imprimervi due canali a forma di serpentino, spaziati al centro da un *plateau*. La membrana funge

invece da supporto per la coltura cellulare e inoltre è l'elemento che subisce la deformazione meccanica e la trasmette alle cellule ad essa adese. Il sistema microfluidico infine serve a garantire il necessario apporto di nutrienti e, eventualmente, segnali chimici alle cellule in coltura. La deformazione avviene diminuendo la pressione lato vetrino in modo da permettere lo scorrimento della membrana all'interno dei canali ricavati nel vetro, ciò determina un aumento della lunghezza complessiva della membrana che viene pertanto stirata.

Le tecnologie adottate nella realizzazione di questo dispositivo annoverano la tecnica di microfabbricazione nota come softlitografia, molto usata in microfluidica grazie alla sua facilità di esecuzione ed economicità, la creazione di membrane elastomeriche sottili e il processo di *wet etching* del vetro. Inoltre si è reso necessario lo studio di sistemi di lubrificazione all'interfaccia vetro-membrana per favorire lo scorrimento di quest'ultima, nello specifico sono stati analizzati due metodi: il primo impiega nanopolveri di teflon come lubrificante solido, mentre il secondo prevede la creazione di uno strato di idrogel lineare che, una volta idratato, favorisce lo scorrimento della membrana. Da studi successivi è stata evidenziata la maggiore efficacia del sistema di lubrificazione con creazione di un menisco artificiale che pertanto è stato l'unico adottato nella realizzazione del dispositivo finale.

I diversi strati che compongono il *chip* microfluidico sono stati analizzati successivamente per ottimizzarne il processo di produzione.

Innanzi tutto è stata analizzata la deformabilità della membrana mediante analisi FEM, correlandola allo spessore della membrana stessa, alla geometria dei canali scavati nel vetro e alla differenza di pressione disponibile, da queste analisi si è scelto di lavorare con membrane spesse 40μm, che rappresentano un buon compromesso tra deformabilità e maneggiabilità della membrana, inoltre si è visto come la deformazione esuli dal campo di idealità, divenendo praticamente nulla per diametri dei canali pari o inferiori a 100μm.

In seguito è stato studiato il processo di wet etching del vetro, in particolare definendo una relazione tra durata della reazione e profondità del canale e ottenendo valori di velocità di *etching* confrontabili con quelli di letteratura. Inoltre è stata studiata, mediante simulazione numerica con il software COMSOL Multiphysics, la morfologia dei canali scavati. Tali risultati sono stati poi validati con una prova sperimentale.

Dalle analisi condotte sulla morfologia superficiale del vetro in seguito al trattamento con acido fluoridrico è stata notata una elevata rugosità nonché la presenza di spigoli vivi alle pareti dei canali scavati nel vetro. Per ridurre ulteriormente l'attrito associato allo scorrimento della membrana elastomerica ed evitare che le sporgenze vetrose danneggino la membrana stessa è stato necessario adottare un processo di ricottura del vetro. Sono state effettuate diverse prove sperimentali per individuare la temperatura ottimale di ricottura, ovvero la temperatura che, pur levigando la superficie del vetro ed eliminando le asperità, preservi la geometria a spirale dei canali realizzati e non ne diminuisca eccessivamente la profondità, è stato notato che a temperature comprese tra 690°C e 710°C si ottiene un buon compromesso tra i due fattori evidenziati.

Al termine di queste analisi è stato possibile realizzare e testare il dispositivo completo. Innanzitutto è stato verificato il corretto svuotamento dei canali scavati nel vetro, tale prova è stata condotta riempiendo i canali con fluoresceina e analizzando al microscopio a fluorescenza la variazione del segnale fluorescente durante la deformazione. È stato notato che i canali del serpentino si svuotano progressivamente dal più periferico fino a raggiungere il centro, in questo modo la geometria a serpentino permette di amplificare la deformazione data da un singolo canale stirando progressivamente la membrana. Inoltre è stato possibile notare il completo svuotamento dei canali, confermando così l'ipotesi che la membrana vada ad aderire completamente al profilo dei canali.
Sono state poi eseguite prove di verifica della deformazione ottenibile marchiando la membrana. risultati preliminari semi-quantitativi indicano il raggiungimento di una deformazione pari a circa il 19%, confermando la funzionalità del dispositivo realizzato, ad ogni modo è stata evidenziata la necessità di realizzare un sistema di marchiatura della membrana più sofisticato, ad esempio inglobando microparticelle solide nella membrana siliconica, in modo da ottenere una mappatura della deformazione ottenuta.
In seguito è stata accertata la biocompatibilità del chip adottato. Il dispositivo microfluidico è stato sterilizzato con etanolo, verificando che tale metodo di sterilizzazione non compromette la successiva coltura cellulare ed infine è stato studiato un protocollo specifico per favorire l'adesione delle cellule in tutta la camera microfluidica. Le cellule in coltura sono state quindi trattate con calceina, un pigmento fluorescente che presenta la peculiarità di essere trasportato attraverso la membrana cellulare delle sole cellule vive e quindi molto usato per accertare la vitalità delle culture cellulari, ed analizzate al microscopio a fluorescenza. Da queste analisi è stata dimostrata la possibilità di realizzare culture cellulari all'interno del chip microfluidico realizzato.

# Index

# Introduction

Recent discoveries in the latest years show that mechanical stimulation could have an enormous importance in the correct development of tissues and organs. Moreover, mechanical defined environment has been correlated with the pathogenesis of skeletal muscle tissues. In this context arises the field of mechanotransduction, which describes the cellular processes that translate mechanical stimuli into biochemical signals, thus enabling cells to adapt to their physical surroundings.

In particular, there is a growing interest in the study of the implications of mechanical stimulation on skeletal muscle cells and cardiac cells *in vitro* with the intent to closely mimic *in vivo* environment. There are two broad categories of research interest that employ mechanic strain: the first one in mainly directed at the study of primary cell differentiation into myocytes and their fusion into polinucleated myofibers and in the functional maturation of cardiac tissue, the second one is intented to study the onset and pathogeneis of muscular or cardiac diseases.

While the first application of mechanical stimulation is aimed at deepen the knowledge of this important biological mechanisms and at allowing an *in vitro* sperimentation more representative of the effective *in vivo* conditions, the latter field shows more direct applications, being designated at the discovery of new targets for muscular and cardiac diseases treatments and at the testing of novel therapies.

In this work a novel microfluidic chip for cyclic biomechanical stimulation of cultured cells is developed and tested. The aim of this device is to allow *real time* analysis at confocal microscopy of cyclically mechanically stimulated cell cultures, improving the currently available technologies that allow only after-treatment analysis or are interfaceable just with standard microscopes. The employment of microfluidic technologies infact enables to realize a compact culturing device with tight control of endogenous or exogenous chemical species.

In the first chapter an overview of the biological research on mechanically stimulated cell cultures is presented, afterwards the current available technology for biomechanostimulation is described and finally the aim of this work is presented.

In the second chapter the conceptual design of the developed device is described, enlightening the characteristic of each single layer that compose the microchip.

In the third chapter the materials and the techniques used in the realization of the device are described, firstly the microfabrication techniques are presented, then the glass wet etching process is exposed and finally the strategies employed to lower friction at glass-silicone interface are reported.

In the fourth chapter the optimization of every layer production and design is outlined. Firstly the membrane deformation is analyzed *via* FEM simulation to explore the strain field and correlate it with membrane thickness and device aspect ratio. Then the glass wet etching process is studied to

determine channel depth correlation with reaction time and final channel morphology, the study was carried out using the software COMSOL Multiphysics, and later some experiments were performed to validate the results. Afterwards the glass softening technique is analyzed to optimize the process temperature. Later on the microfluidic channel geometry is studied using the software COMSOL Multiphysics to compare the fluidodinamic efficiency of different channels geometries. Finally the assembly of the whole device is described.

In the fifth chapter the experimental validation of the microfluidic device is presented. Firstly the fluidic-based control of deformation is tested to verify the correct and complete ejection of liquid from the etched channels in the glass. Finally the device biocompatibility was tested and a seeding protocol was defined.

# Chapter 1
# Introduction and state of the art

In this chapter a brief overview of the current biological application of the developed device will be presented, afterwards the available devices to apply, or methods to simulate, biomechanical stimulation are described, and finally the aim of this thesis work is presented.

## 1.1 Biological application of cell stretching devices

In the current years the idea that the surrounding enviroment greatly affects cells faith and, more importantly, genic expression has establish among the biology field. Mechanotrasduction and mechanical *stimuli* on the cells have proven to play a central role both in cell differentiation and in many signaling pathways that regulate protein production, thus acquiring a central role in scientific research, as the fast increasing number of publications confirms.
More specifically biological research of the stress-stretch cellular response can be divided into two broad areas, focused respectively on skeletal muscle cell differentiation(myogenesis) and cardiac tissue development, and on muscular damage or diseases.

### *1.1.1 Myogenesis*

Myogenesis is a multistep developmental program that generates and regenerates skeletal muscles, thus is required for growth, maintenance and repair of injured muscle fibers.
Pluripotent mesodermal cells, or quiescent satellite cells are activated into cycling myoblasts that subsequently withdraw from the cell cycle and differentiate into plurinucleated myotubes, as shown in figure 1.1

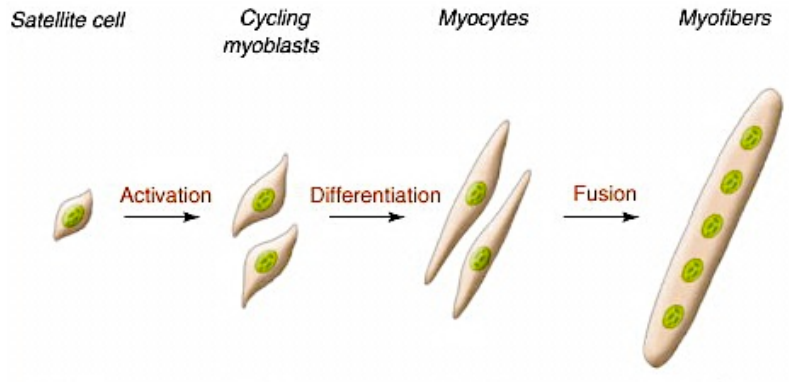


**Figure 1.1** *Schematization of the myogenesis process. First a satellite cell needs to activate into a cycling myoblasts, then the myoblasts differentiate into myocytes and finally the myocytes fuse into a myofiber. Adapted from F. Le Grand and M. A. Rudnicki, 2007.*

More specifically two different phases have been reported to be involved in the conversion of myoblasts into terminally differentiated skeletal fibers: the commitment phase, which requires the

activity of primary myogenic factors such as MyoD and Myf5 for the propagation and survival of myoblasts, and the differentiation phase regulated by the expression of secondary myogenic factors such as myogenin and MRF4. This latter stage is characterized by the synthesis of proteins of the contractile apparatus, sarcomeric myosin and actin, and the fusion of single myoblasts into multinucleated myotubes (Formigli *et al.* 2007).

The fact that mechanical and geometric *stimuli* influence skeletal muscle myogenesis is now well established (Ahmed *et al.* 2009), although the molecular mechanisms are yet to be fully determined, however it is interesting to note that the interaction between external physical forces and myogenesis occurs at many different steps and levels.

Satellite cells, responsible for muscle regeneration following injury and involved in work-induced hypertrophy of muscle fibers, are normally quiescent in adult muscle, however it has been demostrated (Tatsumi *et al*. 2001) that in response to stretch they enter the cell cycle earlier than if they were in static conditions, moreover conditioned medium from stretched cells could activate un-stretched cells as well, suggesting that a signaling pathway that links mechanical perturbation of muscle to satellite cells activation is activated.

Mechanical strain influences also later stages of myogenesis, more specifically several studies have shown that cyclic stretch induces proliferation of myoblasts and inhibits their differentiation into polinucleated myotubes. One of the most frequently proposed signaling pathway responsible for this behavior is p38 MAPK pathway (Kook *et al* 2008 and Hanke *et al.* 2010), that is activated by various external *stimuli* and leads to downstream effect such as transcription factor activation, translation, mRNA stability and chromatin remodeling. Other works suggest the activation of the Rac-1 pathway and of focal adhesion kinase (FAK), that anyways lead to the activation of NF-κB, a protein complex that regulates DNA transcription (Meriane *et al.* 2000 and Kumar *et al*.2004).

Interestingly passive mechanical stress doesn't seem to influence z-line and A bands formation in myotubes, which is the last differentiation step in myogenesis, even though a series of catabolic effects, such as decreased levels of transcription, induction of membrane damage and generation of phospholipase derived products can be detected in muscle (De Deyne 2000).

Finally, mechanical stretch is responsible for the formation of stretch activated channels (SACs) in the cellular matrix that regulate $Ca^{2+}$ influx, intracellular calcium ions trigger many signaling pathways and are recognized to play a central role in muscle differentiation (De Arcangelis *et al.* 2005) and thus might activate selective gene transcription and sarcomeric assembly (Formigli *et al.* 2007).

### *1.1.2 Cardiac tissue development and regeneration*

Cells of the myocardium develop in one of the most mechanically dynamic environment in the body, being subjected continuously to cyclic strain and stress in correspondence to the pulsatile stimuli of chamber filling and emptying. An understanding of cardiac cell micromechanics is therefore a key factor in the design and composition of tissue engineering scaffolds or stem cell niches for further applications in regenerative medicine.

So far it is established that the developing heart needs both mechanical load and vascularization to reach the proper size, moreover mechanical load further controls the hypertrophy and architecture of engineered human myocardium (Tulloch *et al.* 2011).

A critical event for the embryonic morphogenesis of cardiac valves is the endothelial mesenchymal transformation (EMT), that is induced by VEGF, TGF-β1 and wtn/β-catenin and is regulated in a spatiotemporally manner, more specifically a dual-mode strain-dependent EMT has been reported where TGF-β1 signaling triggers EMT under low strain (10%) whereas wnt/β-catenin signaling pathway is activated under high strain conditions (20%) (Balachandran *et al*. 2011). Interestingly, EMT has also been observed in diseased, strain-overloaded valve leaflets suggesting a strain-magnitude and directionally dependent regulatory role of mechanical stress (Balachandran *et al*. 2011).

Mechanical stress plays an important role also in the activation of the renin-angiotensin system (RAS) that mediates both cardiac hypertrophy and heart remodeling. The RAS is an hormone system that regulates blood pressure and fluid balance, all of its components, such as (renin, Ao, ACE, Ang II, Ang II receptors) are present in the myocardium and produced by fibroblasts, recent studies (Verma *et al*. 2010) have shown that mechanical stress activates RAC1 and RhoA which in turn differentially regulate Ao gene expression activating p38 and JNK signaling pathways.

Another effect of cyclic mechanical stress is the self-organization of cardiomyocytes leading to elongated cells orientated transverse to the stretch axis and the enhanced expression of Cx43, an integral membrane protein of the connexin family that seems to be connected to the ERK 1/2 signaling cascade (Salameh *et al*. 2010).

The main concern regarding cardiomyocytes is their application in regenerative medicine, like restoring cardiac function after myocardium infarction. The main issue is that myocytes do not divide in the post embryonic heart so adaptation to meet new mechanical demands and maintain cardiac function is usually achieved by myocyte hypertrophy (Curtis and Russel 2011), a promising solution is the cardiac stem cell therapy (Guan *et al* 2011), though its effectiveness depends on the ability to differentiate stem cells into cardiomyocytes.

### *1.1.3 Muscular damage and diseases*

Mechanical strain plays an important role also on muscle diseases, stretch-induced muscle injury results in the damage that causes reduced force and increases membrane permeability, as a result intracellular proteins leak out of the muscle while extracellular factors might enter the muscle, in this latter case calcium influx seems to be a critical factor due to this ion interaction with may chemical pathways (Allen *et al* 2010).

In the case of Duchenne muscular dystrophy, a severe degenerative disease of muscle which affects approximately 1 every 3500 boys (Dudley *et al*. 2006) with a mutation in the dystrophin gene and commonly leads to patients death within the age of 20, the membrane damage seems to be greater or repaired more slowly (Yeung and Allen 2004, Suchyna and Sachs 2007, Allen *et al* 2010), the reason of this difference, although, are yet to be fully understand.

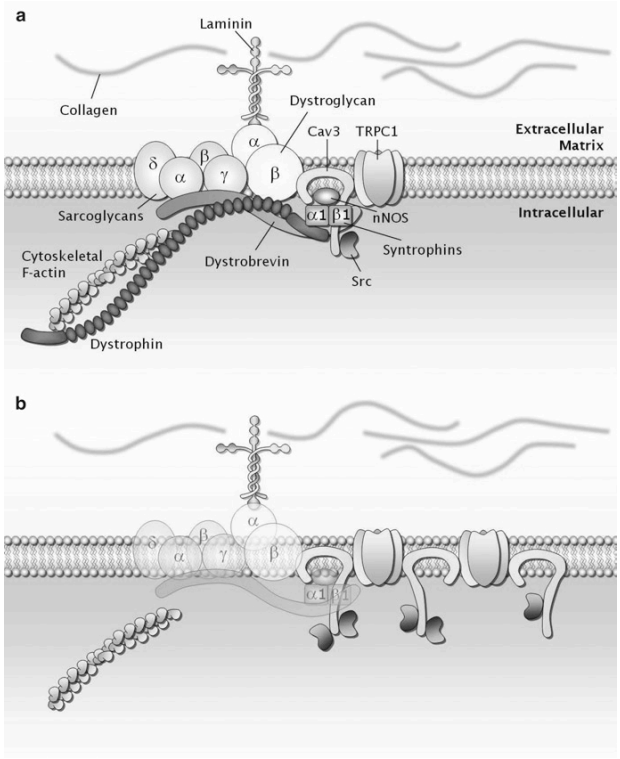


**Figure 1.2***Schematization of the interaction between dystrophin, the dystrophin protein complex and the extracellular matrix in a wild type mouse (a) and in a dystrophic muscle (b). Adapted from Allen et al. 2010).*

The fragility of the sarcolemma, enhanced by the lack of dystophyn, as shown in figure 1.2, is thought to be the primary cause of abnormal stress-induce calcium entry into the cells and therefore to be responsible of the initial damage. The abnormal $Ca^{2+}$ response in mdx myocytes, an mouse model commonly used to study muscular dystrophy, results from the parallel activation of different calcium influx pathways such as stress-activated channels (SACs) and transitory sarcolemma microroptures. Moreover also $Na^{+}$-$Ca^{2+}$ exchange channels (NCX) seems to mediate $Ca^{2+}$ entry subsequent to $Na^{+}$ entry *via* the other pathways, this latter entry pathway isn't prioritary in skeletal muscle, but is likely to be relevant in cardiac muscle where the NCX is highly expressed and active (Fanchaouy *et al.* 2009).

## 1.2 Currently available methods for biomechanical stimulation

Several devices to achieve mechanical stretch of cultured cells have been developed so far, the most commonly used is a commercial device developed by Flexcell® International Corporation (Hillsborough, North Carolina, USA). The Flexcell® device, shown in figure 1.3 employs a circular elastomeric membrane encapsulate in a metal ring and surrounded by an o-ring where vacuum can be applied to deform the membrane itself, the whole system is computer controlled and allows analysis at standard microscopes, anyhow the dimensions of the device prevents its interfaceability with confocal microscopy so its applications are limited.

Another commercially available device is the Stretch Apparatus (Strex) developed by B-Bridge International (Cupertino, California, USA) reported in figure 1.4. In this case a silicone strain

chamber can be deformed along x and y-direction by external mechanical stretch or compression, the culture chamber is interfaceable with fluorescence microscopy.

Other publication report different stretching devices, usually they are achieved by stretching an elastomeric membrane that is fixed in one extremity and connected to a servo motor on the other one (Ahmed *et al* 2009).

A different method for myotubes stretching was propose by Hanke and coworkers (2010) and is schematized in figure 1.5. Basically myocytes are grown on microcarriers suspended in a liquid, during their fusion into myotubes the myocytes extend through different carriers connecting them, when the culture flask is set in a rotary motion, the beads that are at different radial distance from the axis move with different velocities thus stretching the myotubes grown in between them.

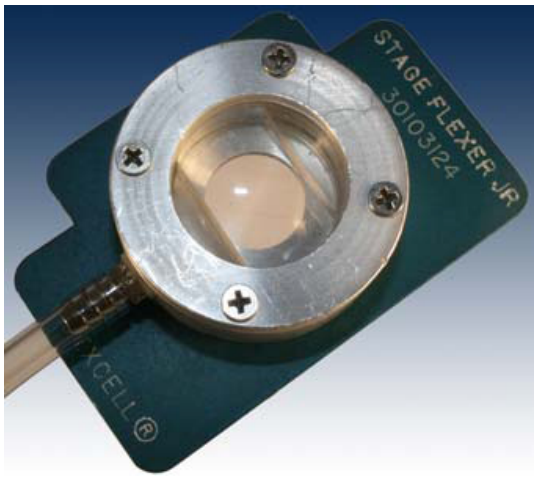


**Figure 1.3***Stage Flexer Jr, developed by Flexcell®* .

**Figure 1.4***Stretch Apparatus (Strex) developed by B-Bridge International.*

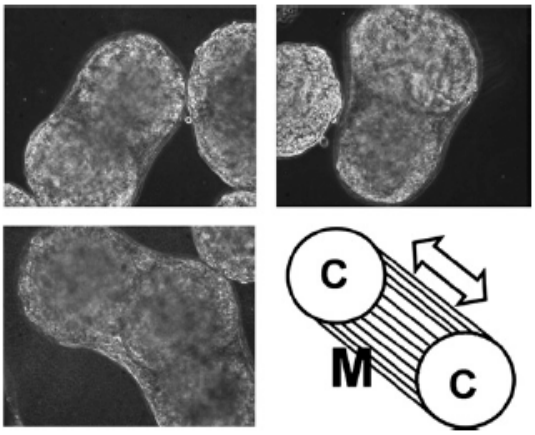


**Figure 1.5** *Stretching device developed by Hanke and coworkers. The myofibers (M) grow across different suspended carriers (C), when the culture flask is stirred, the different velocity of beads situated at different radial positions stretch the cells.*

All this devices share a common flaw: due to their sizes and the need of an external deformation system they are not interfaceable with confocal microscopy, thus severly limitating the analysis can be performed in real time.

## 1.3 Aim of the work

The aim of this work is to develop a novel culturing chamber that allows controlled cyclic biomechanical stimulation of cultured cells, the intention is to create an experimental tool that will deepen the current knowledge in mechanotransduction, to this end the major design specifications are:

- Interfaceability with confocal microscopy (a commonly used instrument for biological research)
- Real time acquisition of mechanically stimulated cell culture with maximum magnification (64x)
- Maintenance of the cellular focal plane
- Achieved deformation of at least 15%
- Close control of colturing conditions

To this end a microfluidic colturing device is designed as described in the following chapter. Later on the conceived microfluidic chip is optimized and realized.

# Chapter 2
## Conceptual design of the microfluidic chip

In this chapter the overall layout of the device and its way of working are described. Moreover the three separate layers by which the chip is made up are analyzed highlighting some key features emerged during the conceptual design.

### 2.1 Device structure and working mechanism

In order to realize a microfluidic platform to cyclically stretch cells cultures that can be interfaced with standard confocal microscopes a three layers device is presented: the top layer consists in a microfluidic channel in a poly(dimethylsiloxane), PDMS, mold and is meant to allow the necessary culture medium exchange and nutrients delivery to cells, the bottom of the channel consist in a PDMS thin membrane on which cells are plated, and finally the bottom layer is made of a microscope slide on which a system of channel is carved. Figure 2.1 represents the three distinct layers.

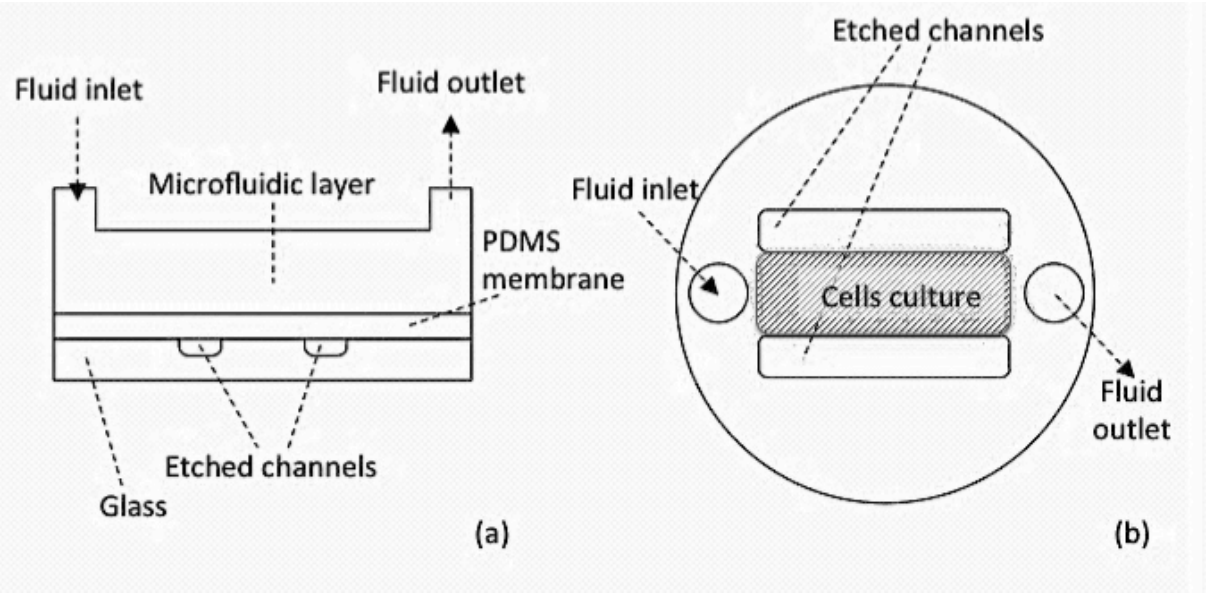


**Figure 2.1** *Outline of the proposed device, the three different layers are enlighten in the front view (a), in the top view (b) the cell culture area is underlined.*

For the device to be used in real time analysis at the maximum magnification available, which is one of the primary goals listed in §1.3, cultured cells must not be further than 200µm from the bottom, this poses a limit to the glass and membrane thickness, whereas the microfluidic system has no limitation regarding its height.

The mechanical stimulation is exerted directly on the elastomeric membrane and transduced to the cells cultured in adhesion on it. Basically the membrane is deformed by creating a pressure difference between its two faces, specifically reducing the pressure on the side facing the glass substrate, thus generating a force that pulls the PDMS membrane inside the channels carved in the glass and stretching it mainly along the transverse direction. The working principle here described is summarized in figure 2.2 where the four major steps are depicted.

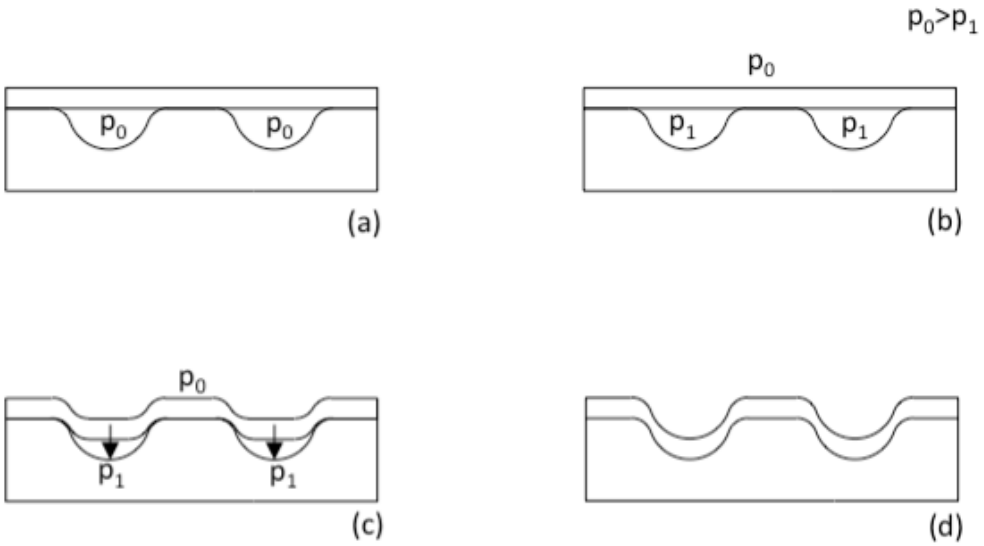


**Figure 2.2** *Schematization of the device working mechanism: a) both side of the membrane are experiencing the same pressure, the membrane is non deformed, b) pressure on the glass side is diminished, c) due to the pressure difference the membrane is pulled into the channels etched in the glass thus being stretched, d) the membrane adheres to the channel's walls, maximum deformation is obtained.*

Two configuration where explored, differing mainly on the fluid used, on the pressure range, which is summarized in table 2.1, and on the lubrication system.

**Table 2.1** *Pressure range used in the two different configuration studied.*

| **Fluid used in the etched channels** | **Pressure on microfluidic system side (bar)** | **Pressure on glass side (bar)** | |
|---|---|---|---|
| | | Basic condition | During deformation |
| Air | 1 | 1 | 0.5 |
| Water | 1.5 | 1.5 | 1 |

The first configuration employs air as working fluid inside the wet etched channels in the glass and the pressure range is between ambient pressure (1 bar) and 0.5 bar, whereas the second configuration employs water inside the etched channels and works in the range of 1.5-1 bar to avoid

cavitation. Using water as the control-layer fluid, also a syringe pump can be employed to empty the channels and thus deform the membrane.

## 2.2 Microfluidic system

The microfluidic system, which represents the top layer of the chip, is made of PDMS and is meant to deliver the necessary nutrients to cultured cells as well as other chemical signals, moreover, being thicker than the other layers, it provides mechanical strength to the whole device.
This layer doesn't differ from common PDMS molds obtained using softlitography (a production process described in §3.1), anyhow in this case it has also to withstand moderate internal pressure (up to 2 bar) that may be required to deform the membrane.
Two kind of channels, showing different shapes, have been taken into account, the first type, reproduced in figure 2.3a, is a simple oval channel whereas the second one, figure 2.3b, presents two channels leading to a central chamber.

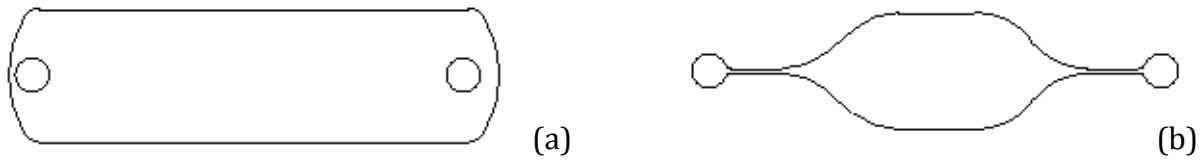


**Figure 2.3** *Top view of the proposed microfluidic channels: a) oval-shaped channel, b) fluidodinamically-shaped channel.*

The first configuration allows a complete overlay of the glass etched channel underneath thus providing a better pressure transduction, on the other hand the flux may be highly irregular, especially close to the inlet and the outlet, compromising the cell culture. The second configuration instead ensures regular flow pathways but doesn't cover the entire length of the underneath channels. A detailed comparison between these two channel shapes is carried out in §4.4.

## 2.3 Membrane

The membrane layer consist in a thin layer of poly(dimethylsiloxane) and accomplishes two key tasks: first of all it serves as a substrate to culture cells in adhesion, secondly it transmits the mechanical stimulation to the cells.
In order to achieve a sensible deformation avoiding the need of large pressure differences, which are difficult to ensure in such a device, the membrane must be thin; a good compromise between deformability and ease of production and manipulation was found to be 40μm of thickness.

## 2.4 Microscopy slide

The microscope slide represents the bottom layer of the chip, in this work two kinds of microscope slides were used: circular microscope slides of diameter 25mm and 100μm thick made in

borosilicate glass and rectangular microscope slides of 75x25mm and µm thick made in borosilicate glass. While the first type of glasses are the one actually used in the final device, the latter were employed in the development of the device for ease of manipulation.
In this microscope slides a series of channels was carved through wet etching with hydrofluoric acid, a technique described in §3.3. Borosilicate glass was chosen since it is easily attacked by the acid yet remains optically transparent.

## 2.4.1 Channel geometry

Not surprisingly the channel geometry was found to be a critical factor defining the maximum membrane deformation achievable, so a preliminary step was to analyze it. Under the hypothesis of ideal deformation, indeed, the maximum deformation, $\varepsilon^{id}$, depends only on the channel aspect ratio and is given by the difference between the deformed length and the one at rest normalized by the length at rest:

$$\varepsilon^{id} = \frac{l_1 - l_0}{l_0} = \frac{\Delta l}{l_0} \tag{1.1}$$

where the symbols used refer to figure 2.4.

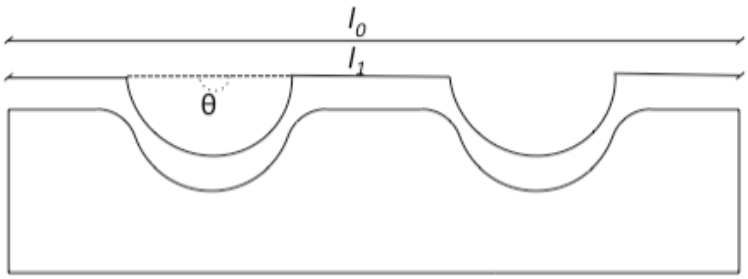


**Figure 2.4** *Schematization of the channel geometry and aspect ratio, $l_0$ is the length at rest, $l_1$ is the length at maximum deformation andθ is the angle subtended by the channel.*

Analyzing the aspect ratio, excluding unfeasible configuration such as an angle θ>180°, the hemispherical channel section (θ=180°) has emerged as the one that could ensure the largest deformation for a given channel depth, as a consequence channel geometry must be designed as to obtain a section as close to hemispherical as possible after the etching process.
Anyhow, the glass slide thickness and the etching technique pose severe limitation on the channel depth, a reasonable value being about 50µm, the resulting maximum deformation, considering a channel spacing of 1mm (the initial value assumed in this work) is about 9.5%, assuming the membrane is bound to the glass immediately at the channel end, versus a desired value of 15%.

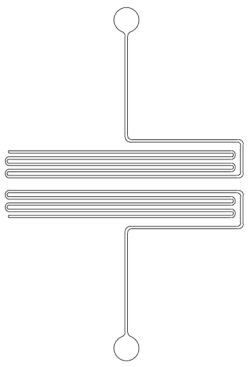

**Figure 2.5***Serpentine-shaped channels employed to enhance the deformation given by channel aspect ratio.*

The solution adopted was to amplify the deformation allowed by a single channel by employing a serpentine shaped channel as shown in figure 2.5. Every bend of the channels multiplies the maximum deformation achievable, on the other hand the distance between two loops decreases the deformation and thus must be minimized.

# Chapter 3
# Materials and methods

In this chapter the materials and the techniques used to design and built the microfluidic chip are described. Firstly the production processes of the three different layers, namely softlitography, thin membrane production and glass wet etching, are outlined, then the techinque used to bind permanently the layers into one piece is presented and finally the methods employed to reduce friction at the glass-membrane interface are presented.

## 3.1 Softlitography

Softlitography is a widely spread technique used to realize microfluidic chips since it allows fast production of micro and nano structures and of rather complex devices yet presenting low costs and ease of production since it is based on replica molding and assembly of different layers into the final product (Xia *et al.* 1998).

Softlitography employs elastomeric materials, the most commonly used being poly(dimethylsiloxane), and, as said before, consist in the molding of the desired structure using a pre-formed, reusable mold. The mold is composed of a rigid substrate, typically a silica wafer or glass, on which the desired pattern is impressed using a photosensible polymer.

Figure 3.1 summarizes the major steps of the softlitography process that will be described in details later on, anyhow it can be noted already that four steps out of six are meant to create the mold so it isn't necessary to perform them every time.

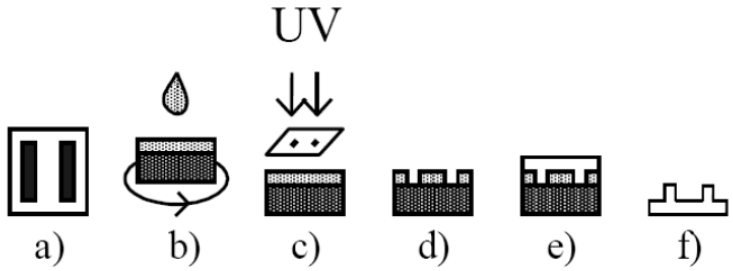


**Figure 3.1** *Schematization of the softlitography process: a) creation of the photomask, b) photopolymer deposition, c) exposure to UV rays, d) development, e) liquid elastomer pouring and thermal curing and f) extraction of the final product.*

The production process evolves into six steps:

- Design of the desired pattern and high-resolution print on a photographic film to obtain a photomask. (figure 3.1a)
- Deposition of the light-sensible polymer, called photoresist, on the substrate and distribution in a homogeneous layer using a spin coater. (figure 3.1b)

- Exposure to ultraviolet light using the photomask to engrave the pattern on the polymer. (figure 3.1c)
- Development of the polymer in a suitable solvent to remove the uncured parts. (figure 3.1d)
- Pouring of the liquid elastomer and thermal cross-linking. (figure 3.1e)
- Extraction of the cured elastomer from the master. (figure 3.1f)

After removal of the elastomer, the mold can be reused many times until the crosslinked polymer starts to detach.

### *3.1.1 Photomask realization*

To obtain the photomask the first step is to design the geometry and draw it using the software AutoCAD 2D (Autodesk), a couple of precautions worth taking are measure units in microns and length accuracy up to the fourth decimal, moreover all angles must be rounded using the command line "*fillet*". During the geometry design it has to be consider that the following high-resolution printing ensures a drawing definition down to 50µm, that therefore has to be taken as the minimum length.

Having drawn the geometry the file must be saved using the ".dwg" extension and later all the parts that have to block UV light, have to be colored in black using Adobe Illustrator.

The drawing can then be printed in high resolution, at least 8000dpi, on the photographic film to obtain the photomask.

### *3.1.2 Polymer deposition*

The second step of the softlitography microfabrication process consist in the deposition of the photosensible polymer on the rigid substrate. The thickness of the layer of polymer determines the final height of the microfluidic features so it must be defined precisely. According to the desired height different polymers, showing various viscosities, are available, moreover the final spin velocities must be tuned according to the polymer used and the chosen height, as shown in figure 3.2.

All the channels of the microfluidc layer used in this work are 100µm high, thus polymer SU8-2050 (Microchem) was employed and all the stages were carried out according to the manufacturer operating manual concerning that specific photoresist.

After the photosensible polymer has been poured onto the substrate all operations must be carried out in complete darkness until the resist is fully developed to avoid light-triggered cross-linking of areas that aren't part of the final geometry.

The polymer is poured onto the substrate, in this work a 4" silica wafer was used, so as to cover about ⅓ of the surface and then distributed homogeneously using a spin coater (Laurell) set to the following two steps program:

1) Spin at 500 rpm with acceleration 100 rpm/s for 5-10s to distribute the polymer along the whole surface
2) Spin at 1700 rpm with acceleration 300 rpm/s for 30s to obtain a 100µm thick layer.

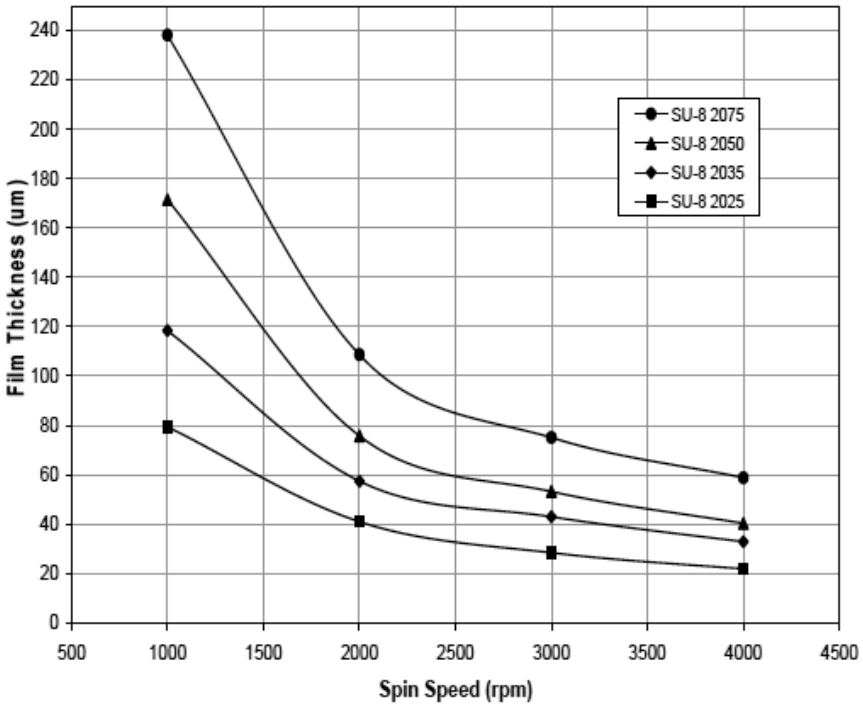


**Figure 3.2** *Photoresist thickness versus final spin speed for different polymers (adapted from Microchem's operating manual).*

Prior to UV ligth exposure a thermal treatment, namely *soft bake*, is required in order to release the inner tensions and allow the evaporation of the solvent.

**Table 3.1** *Soft bake temperature and duration according to the photopolymer thickness (Adapted from Microchem's operating manual).*

| **Thickness** | **Soft Bake Time** | |
|---|---|---|
| (μm) | 65°C (min) | 95°C (min) |
| 100-150 | 5 | 20-30 |
| 160-225 | 5-7 | 30-45 |
| 230-270 | 7 | 45-60 |
| 280-550 | 7-10 | 60-120 |

The soft bake is carried out on a leveled hot plate (Falc), and involves two steps, an optional preheating at 65°C and a second phase at 95°C, the duration of both steps depends on the film thickness as reported in table 3.1.

### *3.1.3 UV light exposure*

After the soft bake the polymer can be exposed to UV light using a AOI lamp that emits a collimated light radiation at the specific wavelength required, namely 365nm, in negative

photoresist, such as the one used, the exposure triggers the cross-linking reaction in the polymer and as a results the geometry drawn in the photomask is transferred to the polymer layer.
The exposure energy, $E_E$ is given by the manufacturer as a function of the polymer thickness, as reported in table 3.2. Knowing the lamp power, P, the required exposure time is given by:

$$t = \frac{E_E}{P} \tag{3.1}$$

where the symbols were described above.
The exposure energy is an important factor, low exposure energy will result in poorly cured photoresist that may dissolve under the action of the solvent, on the other hand, a too high exposure energy may cause crosslinking in parts that should be washed out during the development, especially if the photomask doesn't adhere completely to the polymer during the process.

**Table 3.3** *Exposure energy versus layer thickness (adapted from Microchem's operating manual).*

| **Thickness** (μm) | **Exposure Energy** ($mJ/cm^2$) |
|---|---|
| 100-150 | 240-260 |
| 160-225 | 260-350 |
| 230-270 | 350-370 |
| 280-550 | 370-600 |

During the exposure the lamp power may vary, especially if used for a long time, mainly because of overheating, so its value should be checked frequently during usage modifying the exposure time accordingly.
As said before during the exposure the photomask must be applied to obtain the desired pattern, in order to achieve an high definition in the final mold the mask must adhere completely to the substrate.

### *3.1.4 Development*

After UV exposure and prior to development the photoresist needs a second heating treatment called *post exposure bake* (PEB). Also in this case the manufacturer recommends a two stage process, the first stage, optional, reaches a temperature of 65°C whereas the second one is carried out at 95°C. Post exposure bake time depends upon the polymer thickness as reported in table 3.4.
During PEB a latent image of the pattern should emerge in the uniform polymer layer.

**Table 3.4** *Post exposure bake time as a function of polymer thickness (adapted from Microchem's operating manual)*

| **Thickness** (μm) | **Post Exposure Bake Time** 65°C (min) | 95°C (min) |
|---|---|---|
| 100-150 | 5 | 10-12 |
| 160-225 | 5 | 12-15 |
| 230-270 | 5 | 15-20 |
| 280-550 | 5 | 20-30 |

After the PEB the uncured polymer can be removed *via* a suitable solvent, in this work MF-206 (ROHM and HAAS), a solvent specifically designed for SU8-2050 photoresist, was used.
During the development the wafer is dipped in a Petri dish full of solvent and left there for a few minutes, to speed up the dissolving process the solvent is continuously stirred. In this time the pattern should emerge clearly on the wafer and all the polymer outside the drawn geometry should be washed away. When the development is completed the wafer is extracted and wash with isopropanol (Sigma), if milky-like residues form on the wafer the uncured polymer wasn't removed completely, in such a case it is sufficient to dip again the wafer in the Petri dish for a few more minutes.
Having completed the development process, the mold is left drying in a laminar flux hood until all the chemicals evaporate.

### *3.1.5 Elastomer preparation*

As said before, in this work poly(dimethylsiloxane) was used as the microchip building material. PDMS is a quite common choice in microfluidic application thanks to its high chemical and thermal stability (up to 186°C in air mixture), moisture resistance, high gas permeability, especially to oxygen and carbon dioxide and to its optical transparency down to wavelengths of 300nm that allows UV treatment. Moreover PDMS is a homogeneous and isotropic material and its features can be modified by mechanical manipulation.
The elastomer used was Sylgard 184 (Down Corning), supplied in a standard kit that contains the base, a liquid silicone rubber characterized by end-of-chain vinyl groups, and a curing agent, made of a mixture of a platinum complex and hydroxymethylsiloxane and dimethylsiloxane copolymers.
Base and curing agent can be mixed in different ratios, in this work a 10:1 weight ratio was employed, table 3.4 summarizes the main properties of PDMS obtain using this ratio.

**Table 3.4** *Properties of PDMS in a 10:1 weigth based ratio of base and curing agent prior to (*) or after (**) crosslinking.*

| Propriety | Value |
|---|---|
| Viscosity at 23°C (mPa·s) * | 4000 |
| Passivation time 23°C (ore) * | 2 |
| Tensile strength (MPa) ** | 7.1 |
| Elongation at break point (%) ** | 140 |
| Thermal conductivity coefficient (W/m·K) ** | 0.17 |
| Dielectric strength (kV/mm) ** | 6.5 |
| Permittivity ** | 2.75 |
| Surface tension (dyn/cm)** | 31.6 |

The liquid mixture is prepared in an apposite container mixing thoroughly the two compounds to ensure homogeneity and afterward is put in an hermetically sealed container connected to a vacuum pump, pressure is diminished to about 1 mmHg in order to completely remove air bubbles that may

cause flaws in the final product. Subsequently the liquid silicone mixture is poured on the mold and degassed a second time to remove any air bubble that may have been incorporated. After all bubbles have been eliminated from the liquid, the mold can be put into an oven to speed up the crosslinking process given by the reaction between vinyl, $SiCH=CH_2$, and hydrosilane, SiH, groups. The reaction takes place in 15 minutes at 150°C, 1 hour at 100°C, about 2 hours at 70°C and approximately 24 hours at room temperature.
To ease the subsequent removal of the cured PDMS from the mold the latter is treated with hexamethyldisilazane, HDMS, (Sigma) before adding the liquid silicone. Basically some drops of solvent are poured on the wafer surface and then the mold is put into a vacuum chamber for about one hour to allow HDMS evaporation and homogeneous deposition on the surface.

### *3.1.6 PDMS Extraction*

Once the crosslinking reaction is completed PDMS appears like a solid elastomeric and can be easily extracted from the mold. The extraction is a simple process thanks to the surface treatment with HDMS, usually it is sufficient to delicately lift a corner of the solid silicone to let air penetrate in the interface and afterwards all the mold detaches by pulling the silicone.
The mold can be used again to produce other silicone devices sharing the same geometry, in this case it is sufficient to treat the surface with HDMS just once in a while and anyways after a large number of times.
Also the PDMS mold can be reused for several months without any significative change in its properties.

## 3.2 Thin membranes production

In order to reduce the pressure difference needed to deform the membrane, and thus stretch the cells, of the required amount and to minimize the focal plane translation due to membrane thinning during mechanic sollecitation it is of the utmost importance to obtain a membrane of strictly controlled thickness.
The production of thin layers differs slightly from the softlitography techniques seen before: fist of all the design and realization of a mold is not required since no pattern has to be imprinted, secondly the liquid silicone viscosity must be accurately controlled to tailor spin speed, and as a consequence the film thickness, so a temperature preconditioning is required and, finally, surface treatment to promote detachment is required every time.
The protocol to obtain thin PDMS layers was already defined in F.Michelin master thesis and it comprises seven stages:

- 5” diameter silica wafer surface preconditioning with HDMS for 45 minutes in a vacuum chamber (see §3.1.5)
- Preparation of a silicone base and curing agent mixture in a 10:1 weight ratio (see §3.1.5)
- Pouring of 5.5g of mixture on the wafer and thorough degassing (see §3.1.5)
- Wafer thermal conditioning at 37°C on a pre-heated leveled hotplate

- Achievement of an uniform layer of PDMS of the desired thickness through spin coating
- Curing on a leveled hotplate at 80°C for about one hour
- Extraction of the membrane

Thanks to the thermal preconditioning of the wafer, the final thickness depends only upon spin final speed, the correlation between these two variables was analyzed in Michelin's master thesis and is reported in figure 3.3.

The spin coater performs a two stage process:

1. During the first step, that lasts 5s, the polymer is evenly distributed on the wafer surface, the final speed is 500rpm, acceleration used is 100 rpm/s.
2. During the second step the thickness is defined. Acceleration is 100 rpm/s and the final spin speed is chosen according to figure 3.3, the duration of this step is 1 minute plus the time needed to reach the final spin velocity.

All the membranes produced in this work were 40µm thick so the final spin speed was 1400 rpm.

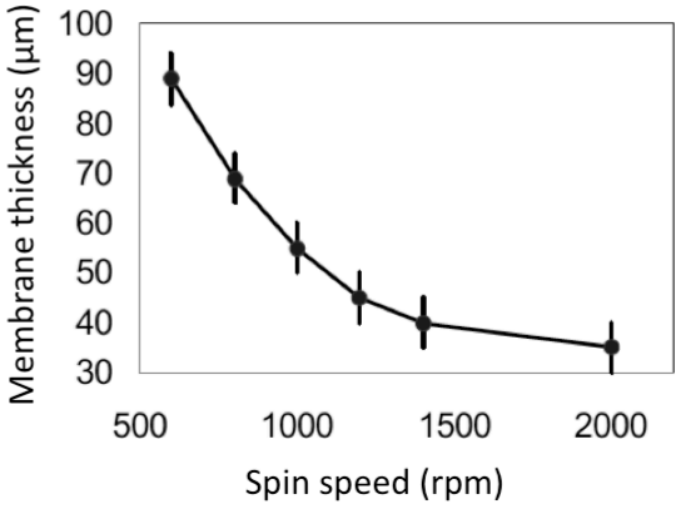


**Figure 3.3** *Membrane thickness versus final spin speed for 10:1 on weight base to curing agent ratio PDMS at 37°C. (Adapted from Michelin, 2010 ).*

Working with very thin membrane the detachment from the wafer must be carried out carefully to avoid damaging the membrane itself. A useful trick is to bond the membrane to the microfluidic layer before removing it from the wafer, this way, infact, the thick microfluidic layer (about 1 cm) enhances the overall mechanical strength and rupture likelihood is greatly diminished.

## 3.3 Glass wet etching

Wet etching consist in carving a fluidic circuit in glass eroding it using hydrofluoric acid. This chemical, in fact, reacts with the silicates which form the core of glass, but is inert with respect to organic compounds, thus the desired pattern can be obtain simply by coating with organic substances all areas that shouldn't be attacked by the acid. In this work positive photoresist, SPR, (ROHM and HAAS) was used to delineate the geometry, whereas the rear of the microscope slide was protected with scotch tape.

Hydrofluoric acid can be used in all concentrations, the higher the concentration the faster is the reaction, in this work hydrofluoric acid in concentration 40% in weight (Sigma) was used.
The wet etching process can be divided into four main phases: photoresist deposition, UV exposure and development to impress the desired pattern on the photoresist, acid attack of the glass and cleaning with piranha solution.

### *3.3.1 Photoresist deposition*

Positive photoresist deposition and processing doesn't differ greatly from the procedure described in §3.1.2÷3.1.4 regarding negative photoresit. The main difference between the two types of resist is that positive photopolymers crosslink thermically and UV exposure degradates the polymer, whereas in negative photoresists crosslinking is triggered by light exposure. As said previously, all operation regarding the photoresist previously to its development must be conducted in completely darkness, being positive resist photodegradable in this case light exposure is extremely harmful.
Also in this case the first step consists in designing and printing on photographic film the desired pattern as described in §3.1.1.
The standard rectangular microscope slides are cut into 25mm·35mm rectangles, whereas circular microscope slides are ready to use, and then washed using "cleaning solution", an apposite detergent that doesn't leave residues, afterwards they are rinsed with demineralized water and left overnight to dry in a laminar flux hood to ensure complete water evaporation.
Afterwards the microscope slides are treated with HDMS for 3 minutes at 130°C to promote polymer adhesion and centered on the spin coater, the photoresit is then poured on the glass slide as to cover about ⅔ of the surface. The spin coater carries out a five step program defined by the manufacturer to obtain a final polymer thickness of 14μm. After deposition is completed, the microscope slides are put on a leveled hot plate at 90°C for 50 minutes to promote photoresist crosslinking.
In order to enhance the photopolymer acid resistance, a key factor in the wet etching process, it's advisable to wait at least 24 hours before exposing the resist to UV light.

### *3.3.2UV rays exposure and development*

The UV light exposure is carried out exactly as describe in §3.1.3, in this case the required exposure energy is 1000 $mJ/cm^2$.
After exposure the polymer is immediately developed using methossimethacrilate (Sigma).
The development is carried out dipping the glass slide in a Petri dish full of solvent and gently oscillating it until the pattern clearly emerges and the parts from which the polymer has to be dethatched appear to be clear glass, afterwards the glass is rinsed with demineralized water and dried with a flux of compressed air. To check whether the development was complete the microscope slide should be analyzed with a microscope (Leica), to spot any trace of uncured polymer on the areas exposed to UV light, if not all the polymer was removed the development process needs to be repeated.

From this point on the polymer can be exposed to light, anyhow, being positive photoresist photodegradable, whenever possible direct exposure should be avoided to assure an high acid resistance.
After development is completed it is suggest to wait 24 hours before hydrofluoric acid treatment.

### *3.3.3 Wet etching*

Wet etching is a very delicate phase of the microfluid chip production process since it requires the use of highly corrosive acids so it is of the utmost importance to employ all the Personal Protective Equipment (PPE) such as suitable gloves, goggles, masks and gowns, moreover all operations must be performed in a laminar flux hood.
Before dipping the glasses in the acid it is necessary to protect also their rear, not covered with the photoresit, with scotch tape. The scotch tape used was chose in order to facilitate its removal after the process is completed.
Having protected accurately all the microscope slides it is possible to start the etching process by dipping the glass in a plastic Petri dish containing hydrofluoric acid at 40% weight based concentration. To maintain an high, and basically constant, acid concentration at the glass surface, thus allowing faster reaction rates, the petri dish is continuously agitated using an oscilloscope (Yellowline, IKA).
The microscope slides where left immerged for about 2’30”-3’, after that period infact part of the protective photopolymer started to detach. The glass slides where washed with demineralized water to remove all hydrofluoric acid traces and then immerged in sulfuric acid at 98% weight based concentration (Sigma) to eliminate etching-reaction byproducts. A second wash with demineralized water followed after which the glass slides where rinsed with acetone (Sigma) to remove the photoresist and the scotch tape. Finally the glasses were washed with demineralized water and air dried.

### *3.3.4 Piranha solution cleaning*

Despite the sulfuric acid wash some residues of the etching reaction may still be present on the etched surface, and they must be removed to maintain the optical transparency of the glass.
Piranha solution is an highly corrosive mixture composed of sulfuric acid at 98% weight based concentration and hydrogen peroxide at 30% weight based concentration (Sigma) in a 3:1 ratio, to maximize its reactivity the piranha solution must be prepared just before usage.
Piranha solution must be prepared and handled in a laminar flux hood since, especially in the initial mixing phase, gaseous hydrogen is formed, moreover it should be remembered that sulfuric acid and water mixing is a highly esotherm reaction, however, after the initial phase when the solution activity is high, the container may be put on a hot plate and heated up to about 60°C to maintain high the reactivity, that otherways will decrease quite quickly.
The etched glasses are dipped inside the piranha solution for a couple of minutes and then washed with demineralized water and dried with an air stream.

## 3.4Plasma bounding

The three layer that compose the microfluidic device are built separately so it is necessary to permanently bound them together, this irreversible bounding is achieved by plasma adhesion, a technique commonly employed in microfabrication processes.

Plasma is an uncharged, partially ionized gas obtained in a plasma cleaner (Harrick Plasma) made of a sealed chamber connected to a vacuum pump in which a constant flux of filtered air is allow to enter in order to keep an internal pressure of approximately 0.3mbar, the entering air is ionized by an intense magnetic field.

The pieces are put inside the chamber with the surface that needs to be attached facing up, the chamber is then closed and the vacuum pump activated. Once the internal pressure reaches 0.3mbar the plasma is activated, when the plasma is formed, which is enlighten by the presence of a purple cloud, the pressure is stabilized to 0.3mbar by slightly opening an apposite valve. Usually two minutes of treatment are required, in this time the ions bombard the surface causing the formation of radicals and thus activating it.

After the plasma treatment is completed the pieces are extracted from the chamber and bound together, a strong binding can immediately be seen due to the reaction between the radicals and the formation of covalent bounds, anyhow, to strengthen the bound, especially if the microfluidic chip has to withstand internal pressure, the piece should be put on a hot plate heated to 100°C (80°C if there's photoresist) for about 30 minutes.

All inlet and outlet ports of the fluidic circuit etched in the glass and of the microfluidic channel must be realized before bonding the PDMS to the glass.

### *3.4.1 Protection of surface portions during plasma treatment*

In the production of the microfluidic chip for cyclic biomechanical stimulations the necessity to avoid binding between PDMS membrane and glass in the central area of the device arises. In fact the membrane must be left free to slide on the glass in correspondence to the fluidic circuit and the cell culture area in order to achieve mechanic deformation, on the other hand, a strong bound between this two layers is required in the outer ring.

To permanently bound just portions of the surface using plasma treatment, all the areas that needed to be free to slide were covered with an acetate film, in this way the plasma ions could not activate that parts of the surface leaving no radicals available to react.

## 3.5 Glass-PDMS interface lubricating systems

One of the main issues regarding the realization of the microfluidic chip is the PDMS membrane sliding on the microscope slide, lowering the friction at this interface would ease the sliding, allowing higher deformations for the given pressure difference of about 0.5 bar.

It has been noted that, despite protecting the surface during plasma treatment, the silicone membrane tends to stick to the glass anyways, and quite strongly, because of chemical affinity. This bound is reversible but affects negatively the device's working since friction is enhanced.

To lower this adhesion tendency two different lubrication systems were studied, in the first case a solid lubricant, namely teflon nanopowders, was employed, whereas in the second configuration an artificial meniscus was created.

### *3.5.1 Solid state lubricant*

The system using teflon nanopowders as solid lubricant employs air as working fluid inside the etched channels, the mechanical stimulation is achieved simply by suctioning the air thus decreasing the pressure in the channels.

A solution of teflon nanopowder in isopropanol is prepared, since this is a physical solution mixing must be energetic and continuous to avoid solids precipitation or segregation.

The solution is suctioned with a pipette and a few dozen microliters are deposited on the central part of the membrane on the side facing the glass. The solution is then gently scrubbed all over the surface with a piece of paper as to evenly distribute the powder, once the solvent is completely evaporated, which requires about 2-3 minutes, the powder depositated outside the central area (the only one that needs to slide) is removed by brushing it with a piece of paper soaked with isopropanol, this step is important since the presence of teflon powder would inhibit the plasma activation of the surface limiting the two layers bounding.

Once teflon is evenly deposited on the PDMS, the membrane can be attached to the glass as described in §3.4.

### *3.5.2 Production of an artificial meniscus*

The second strategy studied to reduce friction at the PDMS-glass interface is the production of an artificial meniscus, more specifically a monolayer of linear hydrogel chemically crosslinked on the glass surface. In this configuration the working fluid is water since the hydrogel needs to swell in order to act as a lubricant, in particular, being hydrogel highly idrophilic and silicone hydrophobic, a thin layer of water is formed at the interface allowing to reduce friction. The entire device is slightly pressurized, at about 2 bar, and deformation is achieved by equilibrating the fluidic ciruit etched in the glass with ambient pressure, in this way the fluid is never depressurized thus avoiding the risk of cavitation.

To create a layer of linear hydrogel first of all the glass surface needs plasma activation (see § 3.4), then a silanizing solution, composed of 950µl of ethanol at 98% concentration (Sigma), 50µl of acetic acid at % (Sigma) and 3µl of (3-aminopropyl)triethossi-silane, is poured on the surface where the hydrogel layer needs to be created, so in this case just on the fluidic circuit and the area comprised among them. The microscope slides are then left drying in a laminar flux hood, after evaporation is completed the glass slides are rinsed with ethanol and eventually dried with a flux of compressed air.

The hydrogel prepolymer can be prepared mixing "*photopattern solution*", APS and TEMED in a 1000:10:1 volumetric ratio. The photopattern solution can be prepared in stocks and stored in a refrigerator, it is composed of 7 ml of *milliQ* water, 2 ml of acrylamide at 4% weight concentration

and 100µl of HEPES at 1M concentration, mixed with 1ml of a solution of 350µg of Irgacure in 1ml of methanol.
The polymeric hydrophilic gel is formed by the chemical reaction of TEMED with the other chemicals, so it has to be added to the solution immediately before usage otherways the gel will form in the preparing container. The prepolymer solution is poured over the glass slides and afterwards other glass slides are pressed over to distribute the drops and obtain a monolayer. After about 20 minutes the reaction is completed so the glass slides can be removed, in order to avoid damage to the hydrogel layer it is advisable to hydrate it prior to detachment.
Before proceeding with plasma bonding to the PDMS layer it is convenient to remove any hydrogel formed outside the desired area otherways it might limit plasma bonding efficiency. In this case it is sufficient to scratch the glass surface with a scalpel.

## 3.6 Glass softening

After the etching reaction the glass surface is very rough enhancing the friction coefficient, moreover the angles of the channels usually are quite acute thus endangering the membrane integrity during sliding, to limit these problems glass softening was studied employing a muffle furnace that allows to reach up to 1000°C with tunable heating rate. Basically the etched glass slides where thermically treated to promote softening, the treatment was carried out heating at 5°C/min, then holding the glass at high temperature for 30 minutes and finally leaving it cooling at room temperature.
Before proceeding with the glass softening it was necessary to treat the glass holder. Earthenware tiles were employed as a bracket, before using they were washed with water to remove any superficial impurity and then they where dried in a stove at 200°C for 24 hours in order to completely eliminate any trace of water. Afterwards the ceramic material was thermally preconditioned by heating it up to 850°C, with a heating rate of 2°C/min, and left for 1 hour at high temperature to assure its resistance during the glass softening treatment.

# Chapter 4
# Technological development

In this chapter key aspect of each layer are analyzed and the device optimization is described.
First of all the membrane deformation range is studied through FEM simulation, secondly the etching process is analyzed focusing in particular on the channel final geometry, then the glass thermal treatment is studied opitimizing the softening temperature and finally the microfluidic layer geometry is analyzed with in respect to both fluidodynamics and pressure transduction.
The chapter is the concluded describing the protocol to realize a complete microfluidic chip for biomechanical stimulations.

## 4.1 Membrane deformation

The thin PDMS membrane is a key feature of the entire microfluidic device here proposed, infact it serves both as a substrate for cell culturing and as the element transmitting the mechanical deformation to the cells.
While thin silicone membrane production is a well consolidated, and already optimized, technique (Michelin 2010), the mechanical stretch of a membrane due to pressure actuation was never investigated, thus a numerical simulation was needed to explore the correlation between driving force (i.e. pressure difference), membrane thickness and its deformability.
All the analysis where performed by professor P. Pavan using FEM simulation, considering a PDMS elastic modulus of 1.8MPa (obtained by previous measurements and a set of single channels etched in the glass distanced 1mm showing an hemispherical cross section. Moreover, to lower computational costs and time axial simmetry was exploited.
The first case scenario investigated assumes a channel radius of 50 μm, membrane thickness of 40μm and a pressure difference of 0.5 bar. In figure 4.1 the resulting deformation is reported, it can be seen that the deformation obtained greatly deviates from the ideal deformation assumed during the preliminary computations carried out to assess the maximum deformation achievable (§2.4.1); in this case infact the stretching isn't linearly distributed along the membrane length but it's concentrated in proximity of the channel edge, giving a deformation of about 11%, whereas in the middle of the membrane, where the cell would be plated and thus stretching is required, the mechanical stimulation is almost unperceivable being the deformation of just 5%. Moreover in this configuration the pressure difference available isn't sufficient to completely deform the membrane, most likely the channel width isn't sufficient and thus the mechanical resistance of the membrane is high enough to compensate the pressure difference.

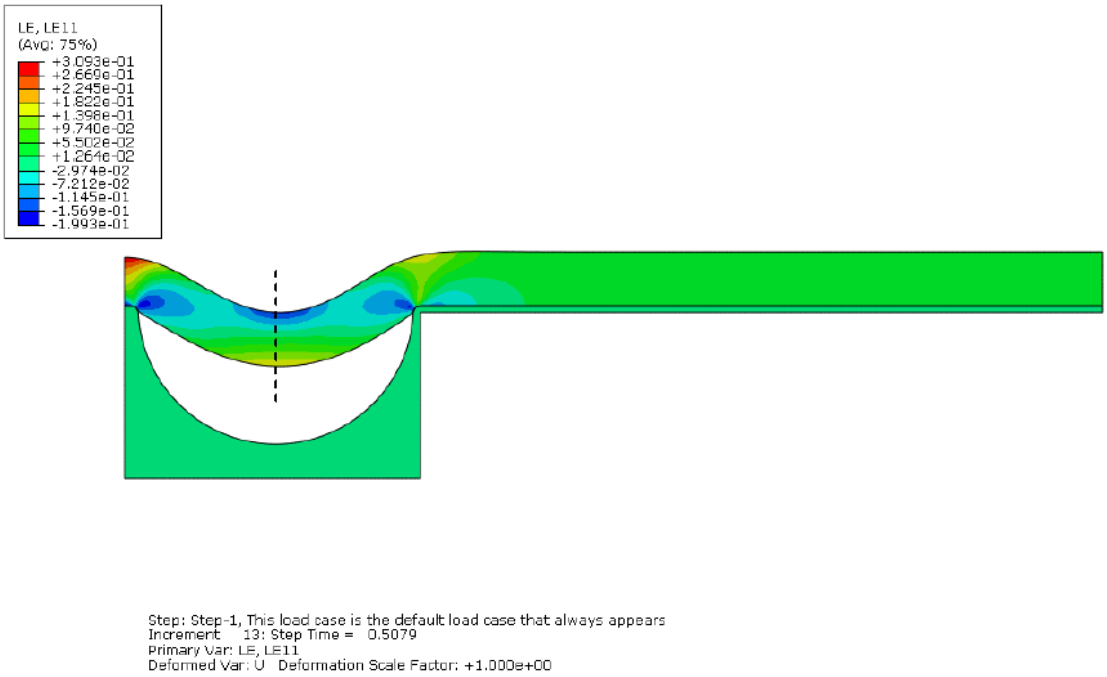


**Figure 4.1** *Membrane deformation field obtained with Δp = 0.5bar and membrane thickness of 40μm in an hemispherical channel of radius 50μm. It can be seen that in the linear part, where the cells will be plated, the deformation achieved is about 5%.*

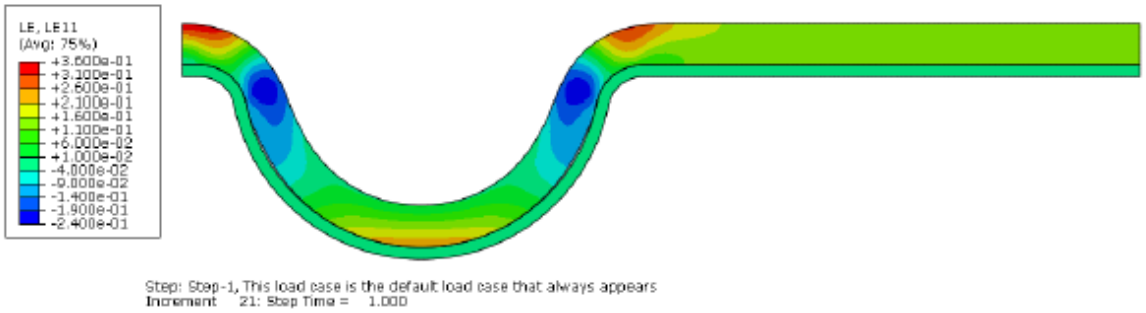


**Figure 4.2** *Membrane deformation field obtained with Δp = 1bar and membrane thickness of 40μm in an hemispherical channel of radius 150μm. It can be seen that in the linear part the deformation achieved is about 16.7%.*

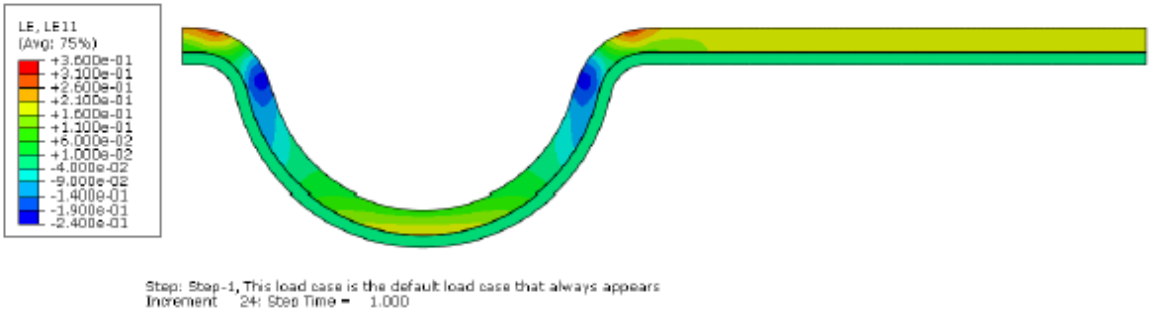


**Figure 4.3** *Membrane deformation field obtained with Δp = 0.62bar and membrane thickness of 24μm in an hemispherical channel of radius 150μm. It can be seen that in the linear part the deformation achieved is about 17%.*

Considering wider channels, more specifically hemispherical channels showing a radius of 150μm, the deformation achieved is higher and more homogeneously distributed along the membrane length, anyhow a pressure difference of 0.5bar isn't yet sufficient to completely deform the membrane, ie the membrane completely adheres to etched channel profile. Regarding this configuration two simulations were performed varying the membrane thickness. In the first case, figure 4.2, a membrane thickness of 40μm was considered, complete deformation is achieved employing a pressure difference of 1bar and the stretching thus obtained in the central portion of the membrane is about 16.7%. In the second case, figure 4.3, a membrane thickness of 24μm was considered, the pressure difference required for the membrane to completely adhere to the glass profile is 0.62bar and the deformation achieved in the linear part of the stretching device is about 17%.

From this analysis the necessity to work under pressure emerges clearly since driving forces higher than 0.5bar are required in any configuration. Another issue arising is the necessity to work with channel depth of 150μm in order to obtain the desired deformation, infact the wet etching technique used to carve the channels, and more specifically the protective photoresist layer resistance, limit the channel depth to approximately 80μm thus confirming the necessity of employing a serpentine channel to amplify the deformation obtained as anticipated in §2.4.1.

## 4.2 Glass wet etching

Etched channels morphology greatly influences both membrane deformability and the maximum deformation achievable, along with channel depth, so it is important to study, and possibly control, the channels final geometry.

To link channel depth and etching time a monodimensional model was developed, while channel morphology was analyzed *via* numerical simulation of the etching process using the software Comsol Multiphysics. The results thus obtained where later compared with experimental measures to verify the models accuracy.

### *4.2.1 Etching depth*

The correlation between etching time and channel depth was already studied in Michelin's master thesis (Michelin 2010) using the same reaction conditions employed in this work, namely hydrofluoric acid concentration of 40% weight based and continuously stirred reaction system using an oscilloscope. In figure 4.4 the channel depth at two different time points, 5 and 10 minutes, is reported. It can be seen that, at least in the time span considered, the correlation appears to be linear.

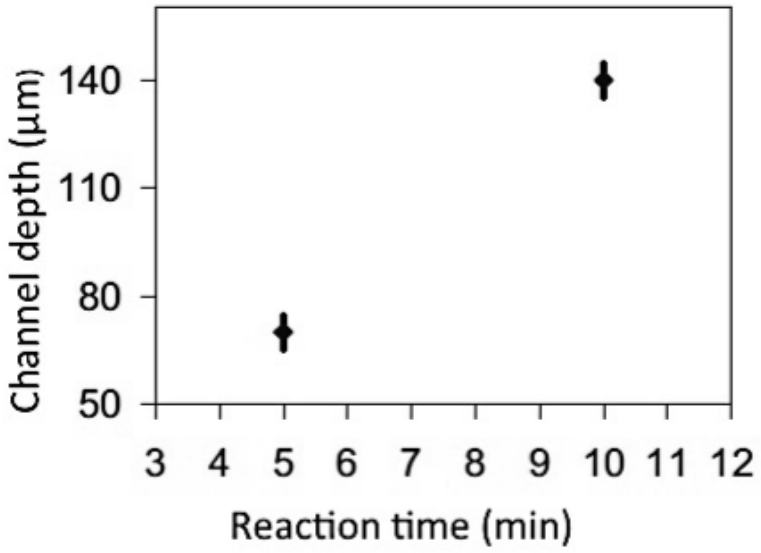


**Figure 4.4** *Channel depth versus etching time using hydrofluoric acid at 40% weighted concentration in a continuously stirred reaction system. Experimental data are taken after 5 and 10 minutes of reaction (adapted from Michelin 2010).*

More precisely the etching rate is determined by the slowest phenomenon between the actual etching reaction and the reactant diffusion form the bulk of the fluid to the glass surface. Anyhow, at small reaction time, ie when the channel depth is limited, being the reaction system well mixed, the reaction rate can be assumed as the rate limiting step (Monk *et al.* 1992) and the acid surface concentration can be assumed equal to the one in the bulk. Moreover, always considering small reaction times, the hydrofluoric acid concentration can be assumed constant since it is available in large excess thus obtaining a constant etching rate as confirmed by the experimental data shown in figure 4.4. Therefore the etching rate can be immediately deduced as the slope of the line passing through the two experimental points, obtaining $v_{etching} = 14 \mu m/min$, a value comparable to those reported in literature (Iliescu *et al.* 2007).
The monodimensional model derived is:

$$\delta = v_{etching} \cdot t \tag{4.1}$$

where δ is the maximum channel depth in microns, and *t* is the etching time expressed in minutes.

### *4.2.2 Channel morphology*

As said before channel morphology greatly affects the microfluidic chip for biomechanical stimulation well functioning, more specifically it is important to define the channel aspect ratio and the walls roughness, avoiding the presence of sharp edges that enhance friction and may damage the membrane.

Since glass is an amorphous material, wet etching is typically an isotropic process (Zhu *et al.* 2009) and the channel profile should be rounded and symmetric with in respect to the channel center, anyhow a numerical simulation was carried out to verify the theoretical trend of the etching process. The analyzed geometry simplified and presents two domains: the fluidic domain, represented in white in figure 4.5, that acts as an acid reservoir, and the glass domain, represented in black in figure 4.5.

**Figure 4.5** *Representation of the geometry used in the numerical simulation using the software Comsol Multiphysics. The hydrofluoric acid a 40% weighted concentration is represented in white whereas the glass subdomain is depicted in black.*

The simulation was solved using the moving mesh (ALE) equations, and the chemical species conservation equation for the hydrofluoric acid.
With regard to the ALE model both subdomains were set free to move according to boundary conditions. The boundary conditions are zero displacement on all boundaries with the exception of a 200μm long central portion of the interface where a displacement rate according to equation 4.1 was imposed.
The chemical species conservation equation was solved only in the fluidic domain, assuming that the acid can not penetrate in the glass but only react with it.
Hydrofluoric acid initial concentration was set to 23M, equal to a weight based concentration of 40%. Boundaries conditions of insulation-symmetry were imposed on all boundaries with the exception of the etched surface where an outward flux of acid was considered to account for the reaction. The hydrofluoric acid consumption due to the etching reaction was calculated as:

$$N_{HF} = v_{etching} \cdot 10^{-6} \cdot \tilde{\rho} \cdot \nu_{HF} \tag{4.2}$$

where $N_{HF}$ is the acid consumption expressed in, $v_{etching}$ is the etching rate expressed in μm/s, $\tilde{\rho}$ is the glass molar density expressed in mol/m$^3$ and $\nu_{hf}$ is the stoichiometric coefficient of the acid in the etching reaction which is equal to 6.
The diffusion coefficient considered is 3.5 10$^{-9}$ m$^2$/s, a value that accounts also for the resistance to diffusion offered by the reaction byproducts, as reported in literature (Monk *et al.* 1992).


**Figure 4.6** *Results of the numerical simulation of the glass wet etching process, the white domain represents the hydrofluoric acid concentration whereas the black domain is the glass. Different reaction time are reported: a) 100s, b) 200s, c) 300s, d) 400s, e) 500 s and f) 600s.*

The numerical simulation confirmed the hypothesis of constant acid concentration used in §4.2.1 since after 10 minutes of reaction the hydrofluoric acid concentration at the reacting surface is 39.57%. The simulation results are reported in figure 4.6 at different time point, namely 100s (figure 4.6a), 200s (figure 4.6b), 300s (figure 4.6c), 400s (figure 4.6d), 500s (figure 4.6e) and 600s (figure 4.6f). As expected the longer the reaction time the deepest the channel until reaching a final depth of about 130μm after 10 minutes, in accordance to the results found previously. Moreover the channel profile is quite smooth and symmetric, thus confirming the isotropicity of the process, of course in this simulation glass heterogeneity is not considered so the actual etched channel may present rougher walls.

It must be noted that some numerical problems aroused during the simulation, infact the moving mesh model acts deforming the mesh according to the imposed boundary conditions, for large deformation this may cause the formation of discretisation elements having zero, or even negative, area thus impairing the numerical method. In order to solve for longer reaction times, and therefore depper channels, a coarser mesh must be used, on the other hand though the interface definition is limited by the element size. All the simulations shown in figure 4.6 were carried out using the same mesh, choosen as the finest mesh that allowed to simulate up to 10 minutes reaction times.

### *4.2.3 Experimental validation*

To validate the results obtained with the numerical simulation experimental tests of the wet etching process were performed. The glass slides were prepared as described in §3.3, using a single channel pattern, and left in the hydrofluoric acid bath until the protective photoresist detached, event that would occur after about 3minutes of reaction.

The etched glass slides were analyzed with a fluorescence microscope (Leica) using a 20x magnification. The channel depth was determined as the difference between the stage height at which the bottom of the channel or the top of the glass slide where on focus, these kind a measurement was chosen since its fast and sufficiently accurate for a preliminary analysis. The

average channel depth measured was about 40µm, a value consistent with the etching ratio deduced from figure 4.4.
The channel morphology was analyzed cutting a microscope slide across the etched channel with a diamond blade and observing it with a stereomicroscope (Leica). A section of an etched channel is depicted in figure 4.7, it can be seen that the morphology closely resembles the one predicted by the CFD simulation, in particular the channel's walls are rounded as expected. In the middle of the channel a wide *plateau* can be observed instead of the expected hemispherical cross section, the *plateu* is due to the large ratio between channel width, about 550µm, and depth, about 40µm, most likely if the channel aspect ratio decrease, the central *plateu* would shorten until an hemispherical section is achieved when the aspect ratio reaches the value of 1.

**Figure 4.7** *Cross section of an etched single channel acquired with a stereomicroscope. The channel width is 550µm and its depth, obtained after 3 minutes of reaction, is about 40µm.*

From the image reported in figure 4.7 it can be noted also that, despite the sulfuric acid and *piranha* solution washes, the surface still presents many impurities and irregularities, this indicates a rough surface that may hinder the membrane sliding.
Afterward other glass slides were prepared, imprinting a serpentine pattern similar to the one used in the definitive chip. In this case the photoresist resistance in the acid environment proved to be higher, allowing for reaction time up to 5min.
The etched glass slides were then analyzed with a profilometer (Sensofar Plu Neox) set in the confocal mode with magnification 20x and 100x. Thanks to the longer etching duration the channel depth resulted to be about 80µm, the measured channel width resulted to be 240µm against a designed width of 200µm, the difference between the actual value and the one defined in the pattern is due to a phenomenon known as "under-cutting", that is the corrosion of the edge of the glass protected by the photoresist owing to the diffusing acid towards the interface. This phenomenon is always present in isotropic etching (Zhu *et al.* 2009) and its effects are increased by poor adhesion between the glass and the protective photoresist, so it must be taken into account designing the photomask for the protective layer.
The analysis was carried out on different spots of the serpentine, as shown in figure 4.8, anyways the depth of the channel and its width are the same in all four spots taken into account so it is reasonable to affirm that the fluidic system carved in the glass presents homogeneous features along the whole geometry.

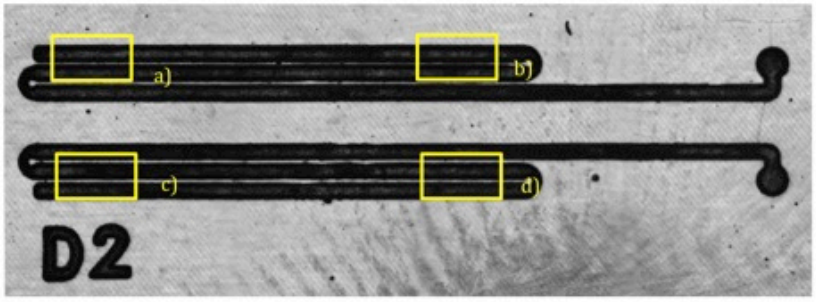


**Figura 4.8** *Top view of the microscope slide with an etched serpentine system analized. The yellow rectangles enlight the spots on whch the measurements were taken.*

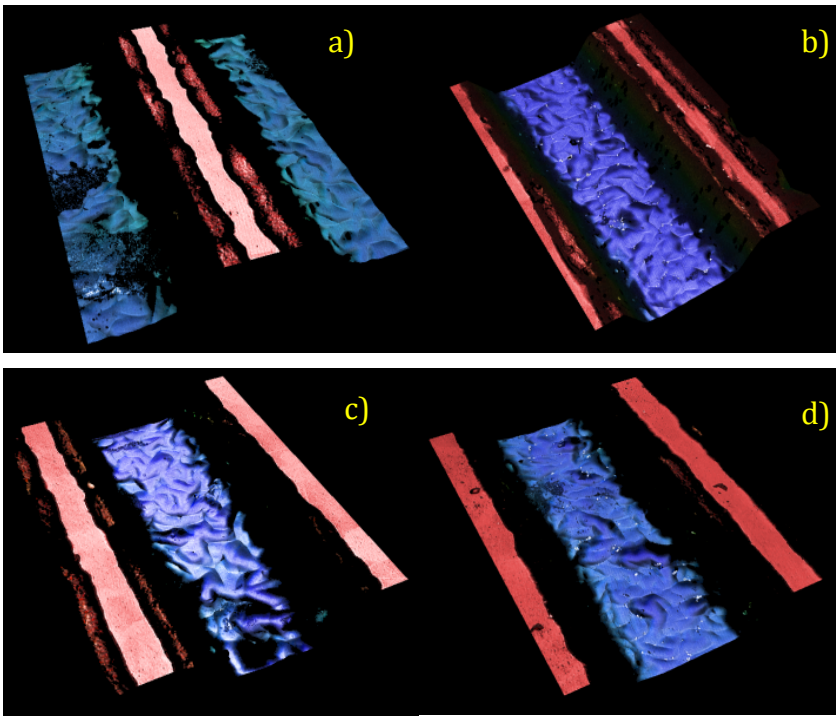


**Figura 4.9** *Results of the characterization of the etched fluidic channels using a profilometer (Sensofar Plu Neox) set in confocal mode with magnification 100x. The letters refers to the four different spot analized as shown in figure 4.8.*

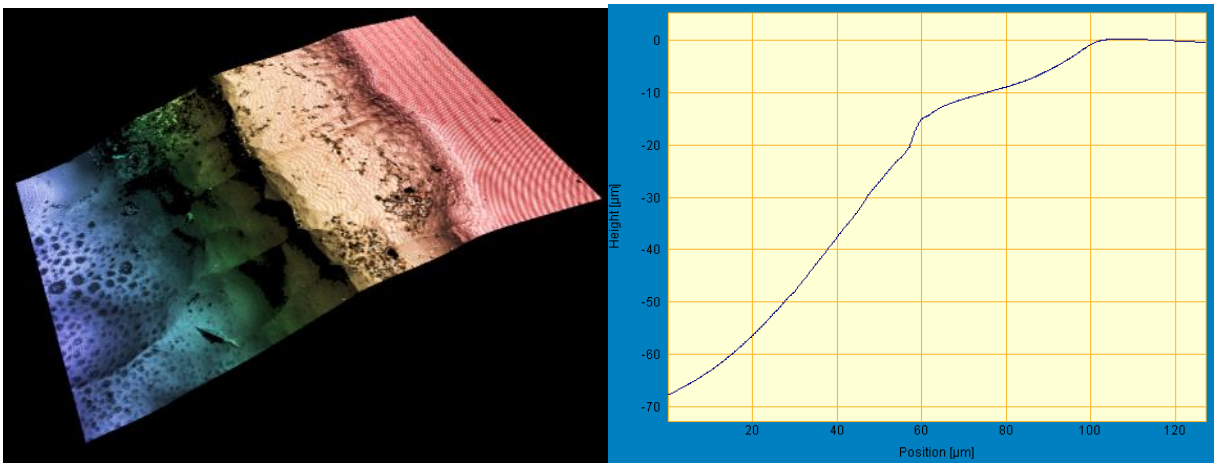


**Figura 4.10** *Analysis of a channel's wall profile obtained inclining the glass slide.*

The results of the profilometer characterization are reported in figure 4.9 for the four different spots, it can be seen that the bottom of the channels is quite rough compared to the top of the glass slide that didn't undergo the etching reaction. Moreover the instrument isn't able to detect the descending channel walls, indicating a quite steep and irregular slope, in order to acquire the walls profile it was necessary to incline the specimens, the result thus obtain is shown in figure 4.9, it can be seen that the slope is fairly circular but the curvature isn't unique and, more importantly, a sharp edge can be detected at the top of the slope, that has to be eliminated to avoid membrane damage.

## 4.3 Analysis of the glass softening process

The characterization carried out in the previous paragrapher enlighten the necessity to smooth the etched channels walls in order to assure a correct working mechanism of the device. To this purpose the glass softening process was studied.

Glass softening consists in a high temperature treatment in which conditions close to the softening point are reached. In such conditions the glass looses its solid-like behaviour and acts as an highly viscous liquid so little imperfections on the surface are eliminated and roughness is greatly reduced. On the other hand the melt-like glass tends to fill the etched channels so an accurate control of the treatment temperature is required.

In order to find an optimal condition between the two phenomenon described several tests have been done working at different temperatures, the treated microscope slides were then analyzed with a profilometer checking both the smoothing achieved and the preservation of the serpentine morphology and channel depth.

In figure 4.11 the different channel profile are confronted, all measure are relative and are meant just to compare the slope shape at different treatment temperature, since the instrument itself isn't able to grant absolute measurements no conclusion can be made on the preservation of the channel depth from this image.

The slope regarding the untreated etched glass, black line, is quite rough and shows a sharp edge towards the top, as the treatment temperature rises the slope becomes smoother. At a softening temperature of 690°C (blue line), the sharpe edges are already blunt, but not completely removed, at 700°C (green line) all sharp edges are eliminated and the walls appear to be smooth, at higher temperature, 710°C (magenta line) and at 720°C (red line), the walls are completely smoothed and the slope is less steep.

From this comparison it can be concluded that the thermal treatment greatly influences the channel's walls profile, as aspected the higher the temperature the greater the effect, anyhow softening temperature of 690°C appreciably diminish the surface roughness while at 700°C the slope is already completely smooth.

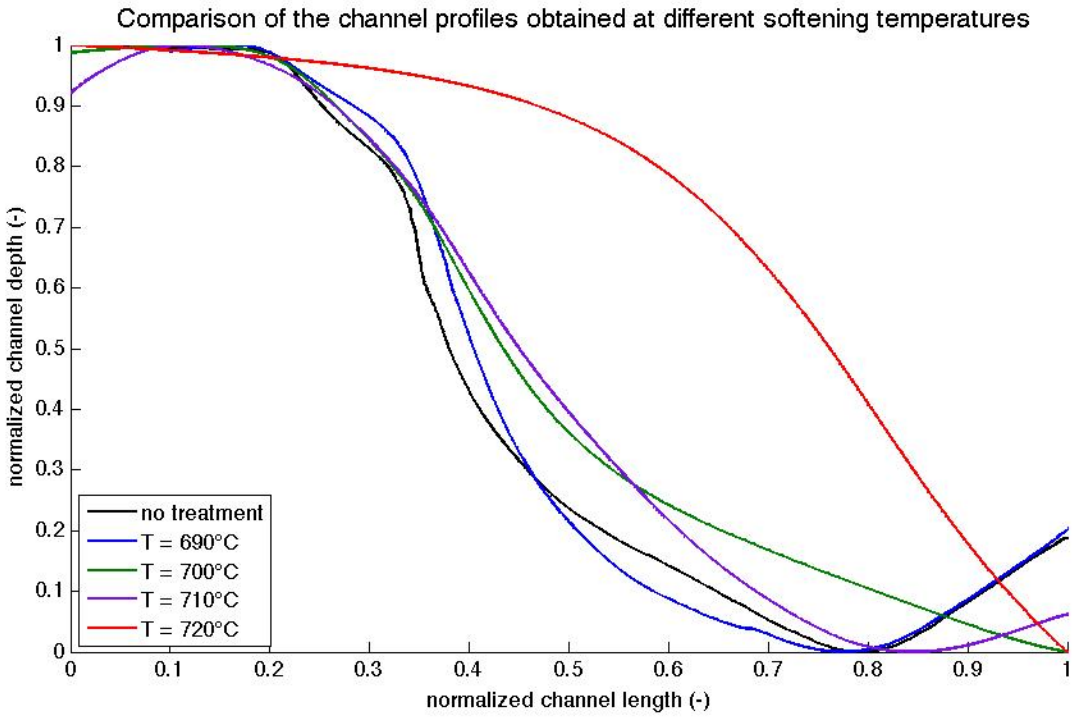


**Figure 4.11** *Comparison of the channel profiles obtain after the etching process (black) or after the softening treatment at 690°C (blue), 700°C (green), 710°C (magenta) and 720°C (red). It can be seen that the higher the softening temperature the smoother the slope, no conclusion can be drawn regarding the serpentine shape preservation since all measures are relative.*

As said before, another important parameter that needs to be considered is the analysis of the softening process is the preservation of the serpentine channel shape, otherways no mechanical deformation can be obtained. In figure 4.12 the serpentine cross section for all the cases described above are reported, a) no thermal treatment, b) softening temperature of 690°C, c) softening temperature of 700°C, d) softening temperature of 710°C and e) softening temperature of 720°C.
From the comparison it can be seen that, up until a temperature of 710°C the serpentine shape is well maintained, and no major differences can be detected in the reported cross sections, at 720°C, instead, the three channels composing the serpentine basically melted together, while the overall channel depth remains constant at about 80µm, clearly in such a case the well functioning of the device is severely compromised.

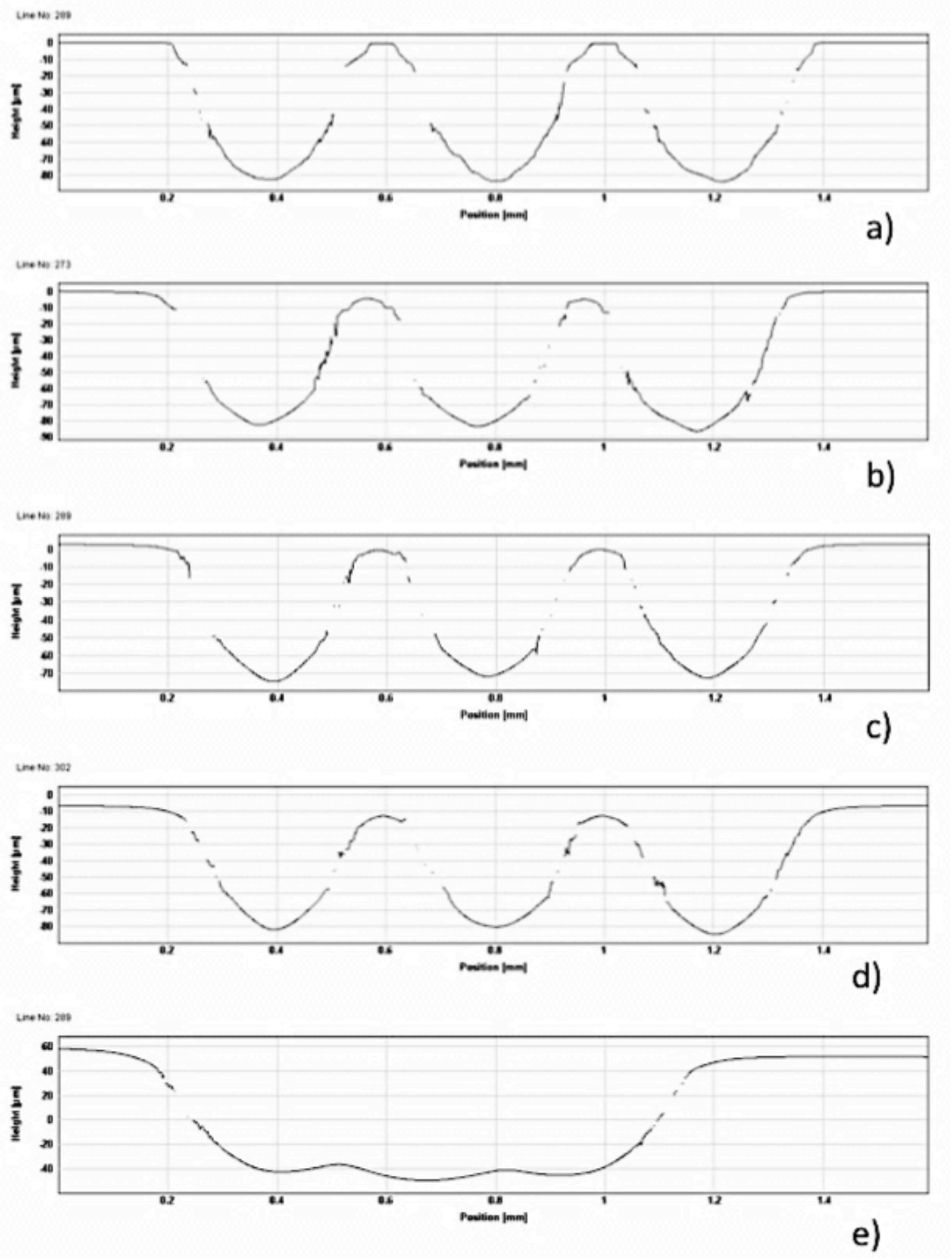


**Figure 4.12** *Cross section of the serpentine shaped channels without thermal treatment (a), and after softening treatment at 690°C (b), 700 °C (c), 710°C (d) and 720°C (e). It can be seen that the channel geometry is well preserved up untill 710°C, and afterwards the structure collapses into one wide channel. Images taken with a 20x magnification.*

The analysis performed on the glass softening process highlighted a viable temperature span ranging from 690°C to 710°C, in fact, as seen, at lower temperature the effect of the treatment is almost null, while at higher temperature the geometry is severely compromised, on the other hand all temperature within the range present similar effects.

## 4.4 Microfluidic layer geometry

The microfluidic layer is the top layer of the device and is intended to confer mechanical strength to the whole microfluidic chip, thanks to its thickness, and, more importantly, to allow the delivery of nutrients and chemical signals to cultured cells and to transduce the pressure on the top face of the membrane.

Two different geometries channel geometries were studied, the first one, oval shaped, intended to cover completely the underneath channels in order to better transduce pressure, the second one designed to optimize the flow pattern inside the channel.

The analysis of the pressure transduction will be presented in the next chapter when the fluid flow in the serpentine is studied, whilst the flow streamlines into the two different geometries were investigated through a CFD simulation using the software COMSOL Multiphysics.

The geometries were directly imported from the CAD file used to design them and simplified by considering the inlet and outlet ports to be on the same plane of the 2D geometry, not orthogonal as will be in real applications.

To obtain the velocity field and streamlines just the Navier-Stokes equations needed to be solved. The boundary conditions used are orthogonal inlet velocity, zero relative pressure at the outlet and no slip condition in all other boundaries. The results are shown in figure 4.13 and 4.14 for the oval channel and for the fluidodinamically shaped one respectively, considering different inlet velocities, namely 0.1 m/s (figures 4.13a and 4.14a), 0.05 m/s (figures 4.13b and 4.14b) and 0.01 m/s (figures 4.13c and 4.14c), anyways all fall within the laminar flow condition.

At $v_{in}$ = 0.1m/s the oval shaped configuration, figure 4.13°, presents high turbulence close to the inlet showing large recirculatory eddies that spread until about half channel, the shaped geometry on the other hand presents a much more orderly flow, figure 4.14°, as indicate by the flow lines that diramates neatly from the inlet port.

Diminishing the inlet velocity to 0.05m/s the oval channel, figure 4.13b, still presents recirculatory eddies due to high turbulence at the inlet, anyhow their extension is reduced to about ¼ of the channel length, for what concerns the profiled channel, figure 4.14b, instead, little difference can be noted, apart from a narrower death layer close to the boundaries.

For inlet velocities of 0.01m/s, or lesser, the flowlines are fairly regular in both the configuration, figures 4.13c and 4.14c, indicating that at Reynolds number close, or smaller, than unity the two geometries are fluidodinamically equal.

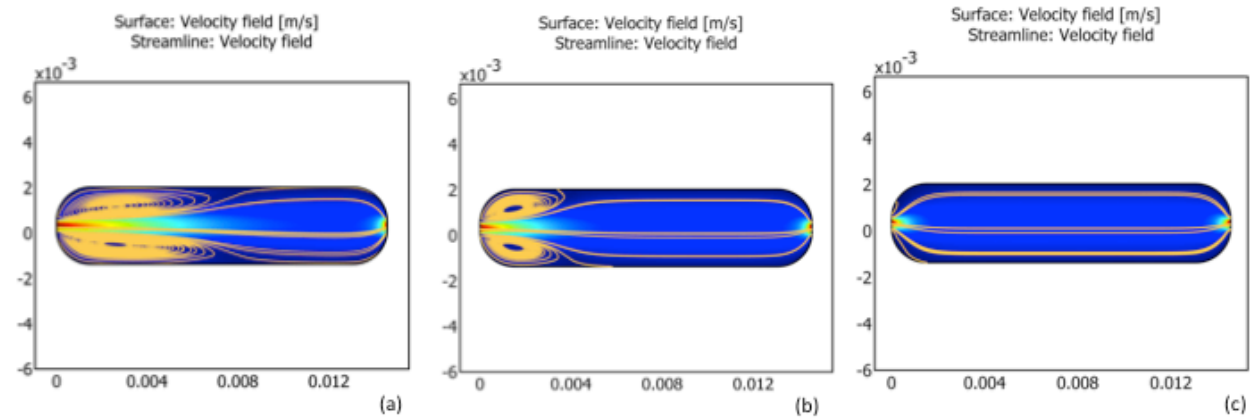


**Figure 4.13** *Velocity field and velocity streamline in the oval shaped channel at different inlet velocities: 0.1 m/s (a), 0.05 m/s (b) and 0.01 m/s (c). As the inlet velocity decrease the flow pattern becomes more regular and recirculatory eddies extension decreases until vanishing at $v_{in}$ 0.01 m/s.*

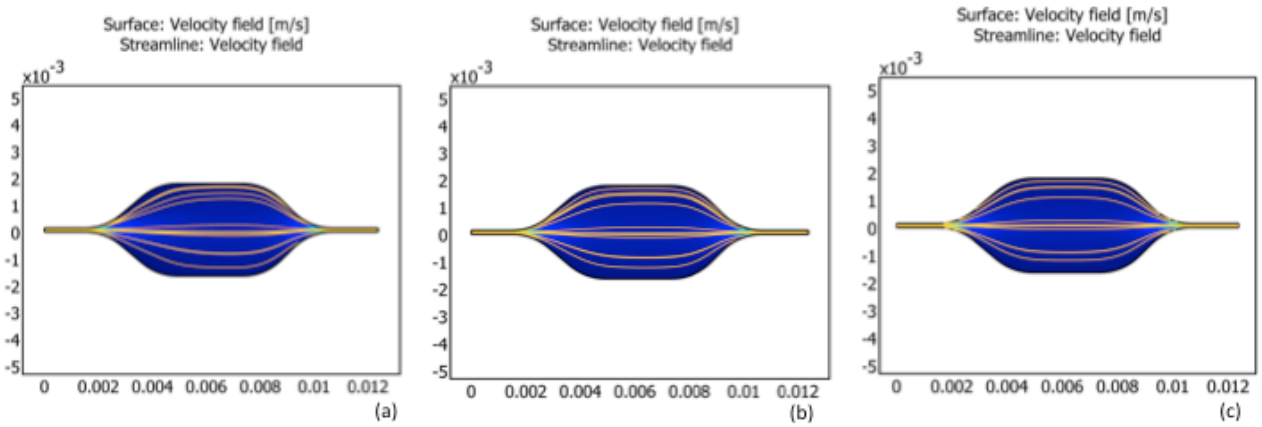


**Figure 4.14** *Velocity field and velocity streamline in the fluidodinamically shaped channel at different inlet velocities: 0.1 m/s (a), 0.05 m/s (b) and 0.01 m/s (c). The streamlines diramate orderly from the inlet at all velocity considered.*

This numerical analysis enabled to find a threshold velocity, at velocity higher than the threshold the two configurations significantly differ in terms of fluidodinamic behaviour and the profiled geometry clearly stands as the best choice, on the other hand, at inlet velocities lower than the threshold, at which Reynolds number is in the order of magnitude of unity, the two configurations are fluidodinamically equal. Since microfluidic applications usually employ inlet velocity in the range of $10^{-3} \div 10^{-4}$ m/s, the choice between the two configuration is irrelevant and can be based on other considerations.

## 4.5 Assembly of the final device

Having analyzed every layer separately and optimized the production procedure the final complete device needs to be assembled. All the techniques needed are described in chapter 3, to which

reference is made for further investigation. The temporal scheme followed, assuming to already have the desired photomask, is:

- First day: microscopy slides cleaning and positive photoresist deposition; production of the geometry on the *wafer* for the microfluidic channels using negative photoresist.
- Second day: UV-light exposure of the microscopy slide to imprint the serpentine geometry on the positive photoresist; realization of the PDMS membrane and of the microfluidic layer.
- Third day: glass wet etching.
- Fourth day: device assembly.

Following this temporal scheme it is possible to optimize the production timing and realize the device in less than a week.

The device assembly is articulated in three main steps: membrane adhesion to the microfluidic layer using plasma surface activation, deposition of the lubrication element and, finally, bounding of the PDMS layers to the microscopy slide. After assembly is completed it is suggested to leave the device on a heating plate at 100°C for about 30 minutes to promote the formation of covalent bounds between the layers.

Before bounding the different layers together it is necessary to perform inlet and outlet holes for the microfluidic channels and for the etched serpentine, this is accomplished puncturing the PDMS with a 1” diameter punch, the inlet and outlets ports for the microfluidic layer have to be realized prior to the binding of this layer with the membrane, whereas those of the serpentine have to be punched just before the binding of the silicon part to the glass. Punched holes are necessary for all the fluidic connection, in this case standard Tygon tubes were employed.

The device is now ready to be used, if the fluid used is a liquid, as in this case, it is advisable to fill all the channels and then slightly pressurize the system to eliminate all gas bubbles, being the PDMS highly permeable to gasses the air is pushed outside due to the pressure difference thus created.

# Chapter 5
# Device characterization

In this chapter the characterization of the device is presented. Firstly the fluidic-based control of the membrane deformation is analyzed, in specific verifying the correct functioning of the serpentine, then a preliminary tests to asses maximum membrane deformation is carried out and finally the biological integration is presented.

## 5.1 Fluidic based control of stretch

The elastomeric membrane is deformed by emptying the serpentine thus allowing it to fill the etched channels and being stretched doing so. To assure a correct functioning the fluid flow during aspiration needs to be studied. Moreover, the serpentine actually improves the total deformation achievable only if the channels are emptied orderly starting from the periphery, infact if the first channels emptied are the ones close to the central area they would act as a pinch point, preventing any further deformation of the membrane placed in the central flat area.

The fluid flow in the channel was studied filling the serpentine with fluorescein, a fluorescent dye, and observing it at fluorescence microscopy (Leica).

Prior to observation air bubbles must be removed from the serpentine otherway they would inflate during the aspiration preventing the correct expulsion of the liquid from the channels. The fluidic circuit, filled with fluorescein, was pressurized to about 0.6 bar and left degassing for about 3 hours, the pressure difference between the two faces of the membrane infact promotes the permeation of air into the PDMS (which is highly gas permeable) and eventually its ejection following the pressure gradient. The serpentine outlets were then connected to a syringe pump (Texas Instruments) equipped with two identical glass syringes (Hamilton) of 250µl, the suctioning flowrate selected was 100µl/min, the microfluidic channel was filled with water and slightly pressurized in order to keep the membrane adherent to the glass surface.

The serpentine emptying phase was analyzed at the fluorescence microscopy with 5x magnification, the results obtained are reported in figure 5.2, only a portion of the serpentine, highlighted in figure 5.1 could be analyzed, anyhow, considering axial symmetry in the system the results are reasonably expected to be the same in all the device.

Figure 5.2a reports the initial conditions of the device, some bubbles can still be spotted but, being so few their presence doesn't pose any problem to the device well functioning, it can be seen that initially the fluorescent dye is evenly distributed in the serpentine. In figure 5.2b the fluid withdrawal is started and it can be seen that the top channel, the furthest from the center, the fluorescent dye is expelled. The fluid ejection from the channels continues neatly in figures 5.2c to 5.2e until all the fluoresceine is eliminated and the serpentine completely black out apart from some residuals that remain at the channels walls.

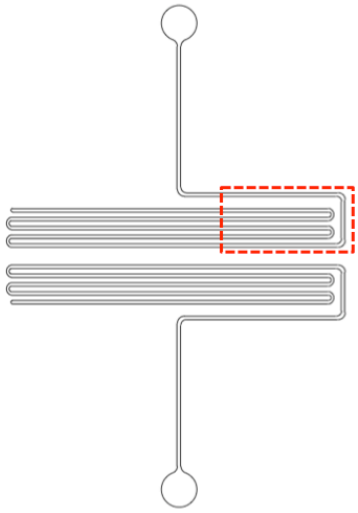

**Figure 5.1***Top view of the serpentine shaped circuit etched in the glass, the red rectangle highlights the area viewed at the fluorescence microscopy .*

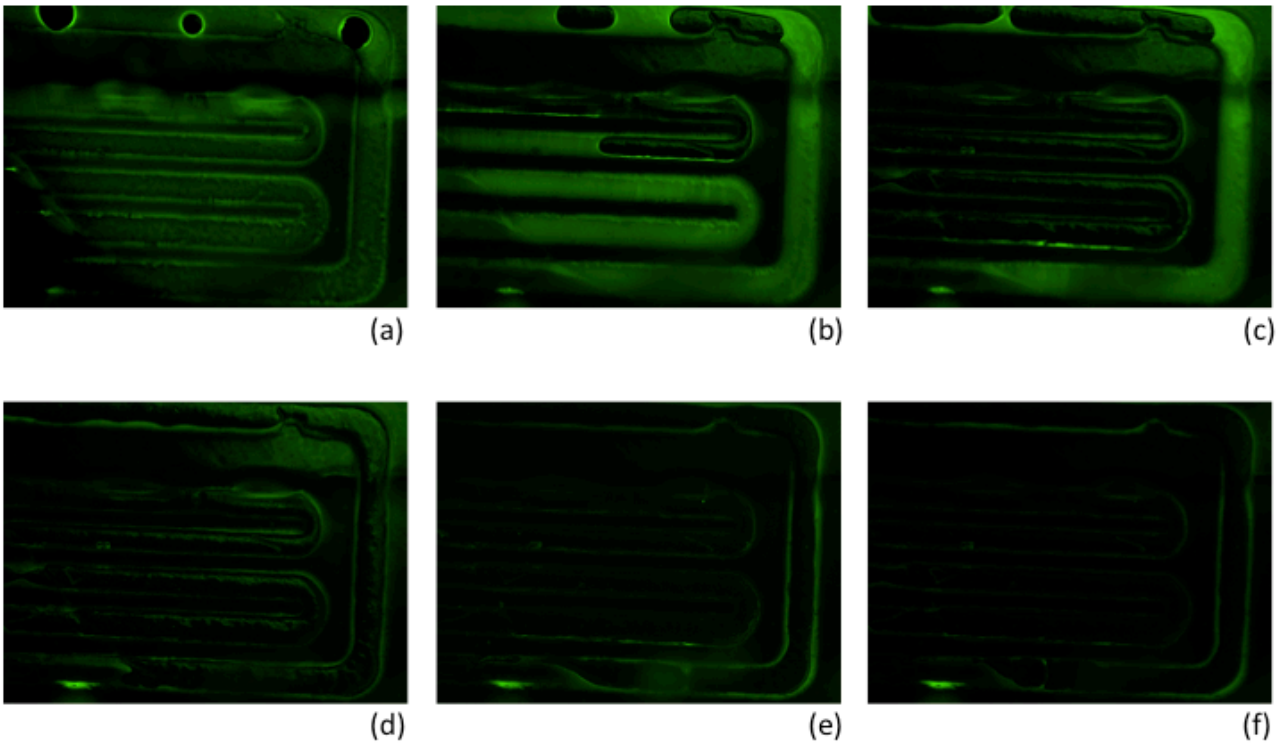


**Figure 5.2***Temporal sequence of the liquid ejection from the serpentine during membrane deformation. The etched channels were filled with a fluorescent dye (a) and then emptied using a syringe pump (b to e) until complete expulsion of fluid (f). It can be seen that the channel is emptied orderly starting from the outer channels, confirming the device well functioning. All photos were obtained with a fluorescence microscopy at 5x magnification.*

The analysis confirmed the correct functioning of the serpentine system, infact the fluid is expelled starting from the outer channel and then towards the center, in this way the membrane is gradually stretched as the serpentine loops are emptied. Furthermore it can be noted that all the liquid is expelled from the channels, figure 5.2f, since basically no fluorescent signal is detected, thus the membrane is free to completely adhere to the glass contour.

## 5.2 Membrane deformation

To assess the amount of deformation allowed by the device several staining techniques have been studied. Firstly the possibility to transfer a ink or fluorescent pattern on the membrane *via* contact printing was analyzed, this technique consists in staining a PDMS mold that presents the desired pattern, in this case a matrix of dots, and then pressing the mold onto the membrane to transfer the dye. Anyhow this method, frequently used to stain glass surfaces, proved to be inefficient in this case to the lack of difference in superficial properties between the membrane and the mold, also plasma activation of the membrane surface didn't improve the transfer efficiency.

An alternative method was to directly stain the membrane with a permanent marker pen, in this case the irregular shape of the stains prevented the use of imaging tools available in Matlab, moreover the ink dots obtained resulted to be too big, frequently as big as (or even bigger than) the central flat area designed for cell stretching, as a consequence the following image processing to assess the deformation obtained proved to be complicated and highly inaccurate.

Slightly better results were obtained by marking the membrane with teflon nanopodwer before it was completely cross linked so the powder would be incorporated on the membrane surface, anyhow also in this case it wasn't possible to obtain a clear pattern so the deformation is calculated subtracting the distance between two random dots before and after deformation and normalizing their difference with respect to initial distance.

In figure 5.3a and 5.2b the frame before and after deformation in the device employing the artificial meniscus as a friction-reducing method are reported, the dots used for the deformation quantification are circled. The deformation was calculated for different couples of points considering just the direction orthogonal to the channel, deformation in the cross direction is due to a non-ideal deformation field derived by the fact that the membrane on the side is attached to the glass immediately after the etched channels and can be eliminated or greatly reduced by allowing space after the end of the channel before attaching the membrane.Processing these images a 19% deformation was calculated confirming that the developed device is able to provide deformations higher than the design specifications requirement of 15%.

A similar test was carried out on the device treated with teflon nanopodwer to lower sliding-associated friction, in this case the observed deformation was inferior so the device employing hydrogel was used in all following experiments.

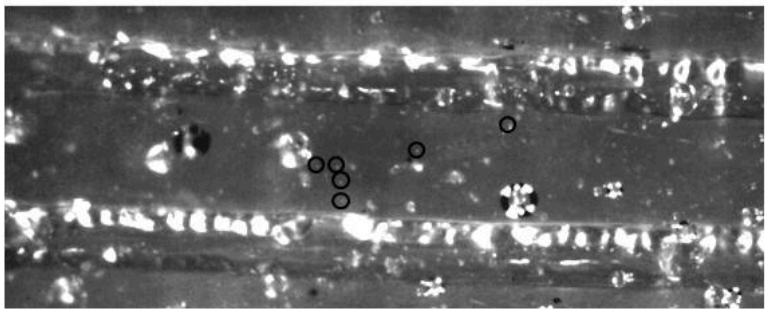

(a)

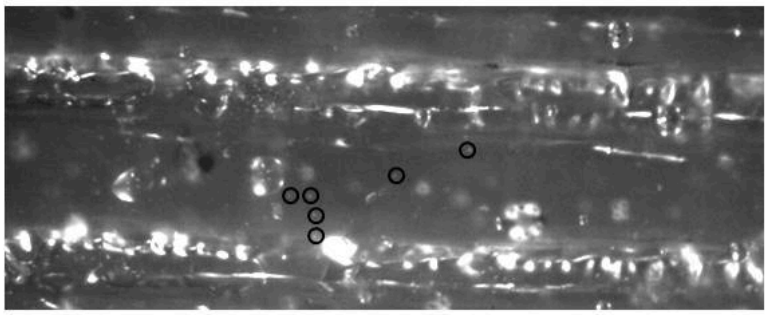

(b)

**Figure 5.3** *Analysis of the deformation obtained with the device employing an hydrogel artificial meniscus to lower sliding friction. The center of the membrane is visualized before (a) and at maximum (b)mechanical stimulation, the deformation achieved is calculated as the difference between the relative distance of two Teflon nanopowder particles (the ones considered are circled) in the two cases and normalizing it by the distance at zero deformation.*

The staining technique used allowed to determine the deformation obtained in the developed device, anyhow it can be seen from figure 5.3 that the analysis is complicated by the lack of resolution in the image and the scarcity of conspicuous reference points.
A more sophisticated staining technique is currently under study, it this case the aim is to incorporate microparticles in the liquid PDMS before spinning it on the silica wafer, anyhow the homogeneous distribution of particles in the membrane isn't easy to achieve.

## 5.3 Biological integration

Having proven the correct working mechanism of the bottom layer, the following step is to assure the device biocompability. Firstly the sterilization technique was analyzed, then the cell seeding protocol was defined and finally a stretching test was performed.

### *5.3.1 Device sterilization*

The common procedure to sterilize microfluidic chip prior to cells seeding is autoclaving, that is treating the device with high temperature steam, usually 121°C. However hydrogel behavior to such a treatment isn't reported, and there is the possibility that it may be degraded so different sterilizing techniques were explored. Other two common sterilization methods are UV treatment and ethanol treatment. The first method is quite simple to use but the thick PDMS that composes the microfluidic layer, while not blocking completely the UV rays, may diminish their efficiency so

ethanol rinse was used. Using ethanol care must be taken since it may inhibit also the subsequent cells adhesion to the surface, so as a first step cells adhesion to the surface was explored firstly observing them in phase contrast, and secondly treating the cells with calcein, a fluorescent dye that can be transported through the cellular membrane into live cells, which makes it useful for testing cell viability, and then observing the cells by fluorescent microscopy.

The ethanol sterilization of the device was carried out by flushing ethanol into the microfluidic channel, where cells will then be seeded, and then, after a couple of minutes, suctioning it from the channel, afterwards the device is left for about half an hour in the biological safety hood to complete evaporate alcohol residuals.

The channel was then filled with gelatin and fibronectin, as described in §5.3.2, to promote cells attachment, afterwards the HHF cells were seeded, along with culture medium, and left in the incubator overnight to allow them enough time to settle to the new environment.

Prior to calcein treatment cells where observed in phase contrast to ensure they were attached to the bottom of the channel, and then calcein, diluted in culture medium at 3µM, was injected in the chamber. After an incubation period of 30 minutes cells were observed at fluorescence microscopy, the results are reported in figure 5.4 and 5.5.

In figure 5.4 the entrance of the culture chamber is depicted both in phase contrast (5.4a) and in fluorescence (5.4b). It can be seen that in this point cells attached quite well to the chamber bottom and are almost uniformly distributed along the channel cross section, the same situation occurred at the other end of the channel (data not shown), anyways it can be also noted that the cells tend to remain close to the channels walls, and the culture is v-shaped at the entrance of the chamber.

This tendency to remain close to the walls is confirmed in figure 5.5 where just a few cells can be spotted all close to the wall while the center of the chamber is completely empty.

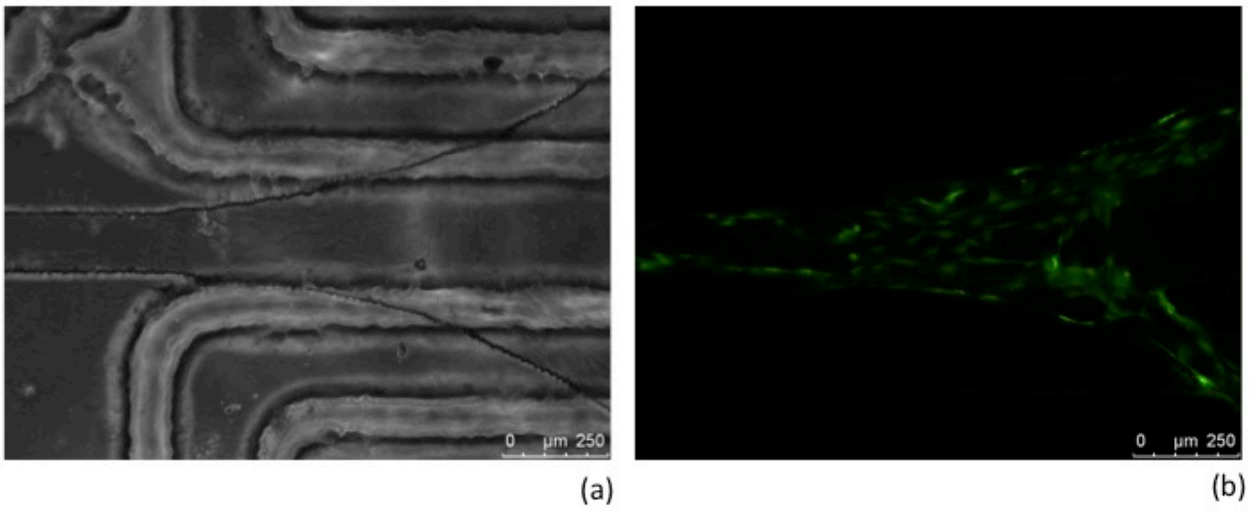


**Figure 5.4** *Cells adhered in the culture channel at the entrance of the chamber. In phase contrast (a) che top layer channel outlines can be seen as well as a portion of the underneath serpentine but it is difficult to spot the cells, in fluorescence (b) only the membrane of live cells can be seen enlighten their presence.*

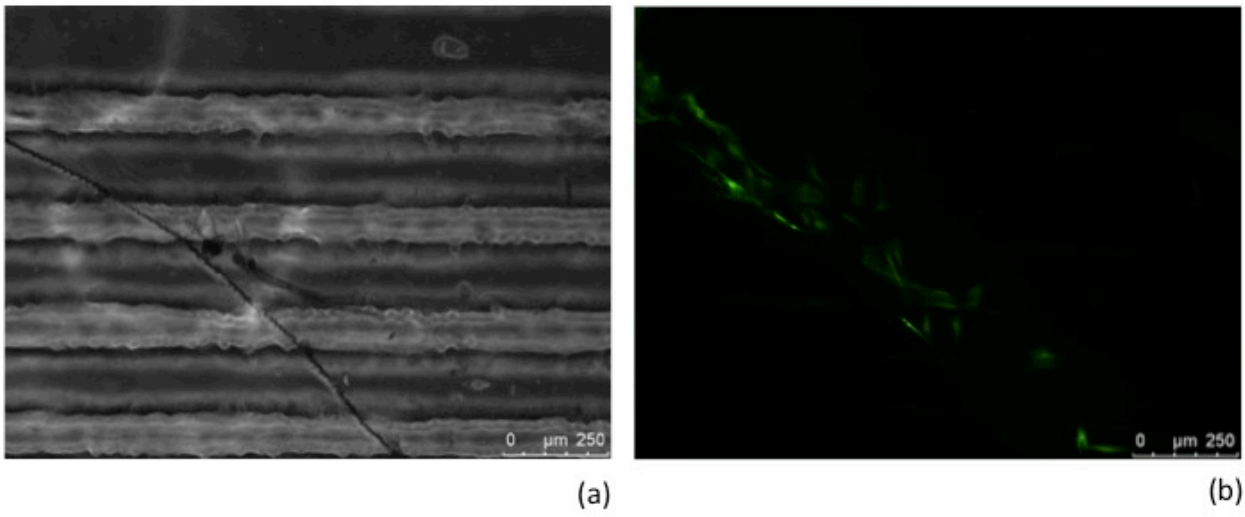


**Figure 5.5** *Cells adhered in the culture channel in the central chamber. In phase contrast (a) the geometry of the underneath serpentine interferes with the cells visualization, in fluorescence (b) only the living cells can be seen and it can be noted that they are present only at the border of the chamber.*

This odd cells distribution in the culture channel can be explained if the membrane is slightly lifted during the seeding procedure, in fact, in such conditions, the center of the membrane, and, therefore, of the culture chamber, will be higher than the rest of the chamber, both adhesion promoters (A-type prok gelatin and fibronectin) would preferentially settle at the lower borders and thus cells will adhere mostly there leaving the center of the chamber empty. Anyways the presence of live cells in the channel confirms that the device can be sterilized with ethanol without compromising the subsequent cell culture.

### *5.2.2 Seeding protocol*

To avoid the selective cells adhesion observed in figure 5.5 a seeding protocol that takes into account the necessity to flatten the bottom of the culture chamber was developed.

The microfluidic device was sterilized with ethanol, after alcohol complete evaporation the serpentine was filled with PBS, used instead of water to provide an isotonic environment on the two faces of the PDMS membrane, the serpentine was then slightly depressurized to promote membrane adhesion to the glass surface at the center, and left so until cells adhered to the membrane.

Then 0.66% A-type pork gelatin (Sigma-Aldrich) was flushed into the culture channel and left for 90 minutes, afterwards the residual gelatin was suctioned and the channel was filled with fibronectin (BD). After waiting for another 2h the residual fibronectin was suctioned and cells were seeded along with culture medium composed of 89% DMEM (1 g/L glucose) (Sigma-Aldrich), 10% FBS (Invitrogen) and 1% penicillin/streptomycin (Invitrogen). Cells were cultured at 37°C with 5% of $CO_2$ to provide optimal conditions.

After this seeding procedure the cells where observed in phase contrast throughout the chamber length, as reported in figure 5.7 in this case the cells are present also in the culture chamber confirming the success of this seeding protocol.

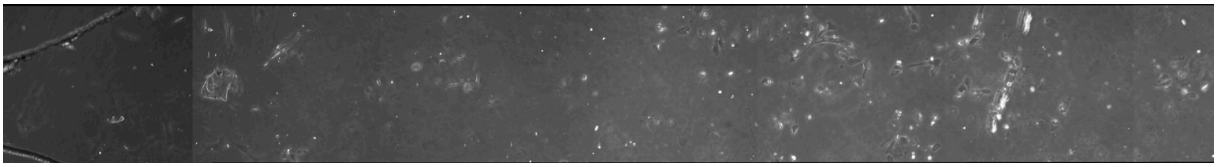

**Figure 5.6** *View of the culture channel. After improving the seeding procedure cells are seeded along all the chamber h*

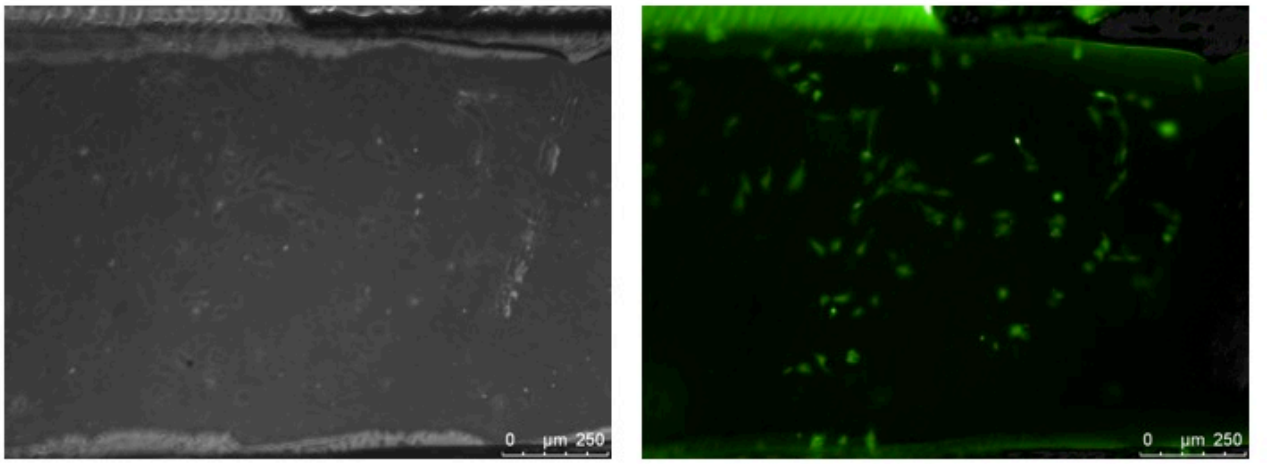


**Figure 5.7** *View of the center of the culture channel. Seeded cells can be seen both in phase contrast (a) and in fluorescence (b), the green staining of cultured cells proves their vitality. Images taken with a fluorescence microscopy at 20x magnification.*

Also a cells vitality test has been performed using calcein as previously described, in figure 5.7 the image taken with fluorescence microscopy at 20x magnification is reported, the presence of green stained cells proves that it was possible to successfully seed and keep alive cells in the center of the channel, setting the stage for subsequent cells stretching experiments.

# Conclusions

Biomechanotrasduction is a fast growing field of biological research, mechanical forces are infact converted by cells into chemical signals and thus influence tissues and organs formation, cell differentiation and gene expression and are closely related to many pathological condition of muscle and cardiac tissues.

The ability to recreate a *in vivo*-like mechanically active environment for cultured cells is therefore of the utmost importance for many research areas: it allows to study myogenesis and cardiac tissue formation, to get an insight of many signaling pathways activated by mechanical stress in muscle and cardiac cells and to explore new targets and test therapies for common diseases, such as Duchenne muscular dystrophy or myocardium infarction.

In this work a microfluidic device for cyclic biomechanical stimulation was developed, the peculiarity of this microfluidic chip is that it allows real time analysis of stretched cells using confocal microscopy, thus enabling the study of transient phenomenon such as calcium influx due to stress activated channels opening and membrane microruptures.

The proposed device is composed of three layers: a microscopy slide in which a couple of serpentine-shaped channels are etched, an elastomeric thin membrane, on which cells are cultured and that endures the actual mechanical deformation, and a microfluidic channel, that enables the delivery of nutrients and, if necessary, chemical *stimuli* to the cultured cells.

Every layer design and production were analyzed separately and optimized in order to achieve a deformation of at least 15% and to optimize culturing conditions. Moreover the interface between the glass and the elastomeric membrane was lubricated by creating an artificial meniscus, made of linear hydrogel, to lower the friction associated with the membrane sliding during deformation. For the same reason and to eliminate sharp edges that may damage the membrane, the glass softening process was studied to find an optimal process temperature that allows surface smoothening yet preserving the channel geometry.

Finally the complete device was assembled and tested. Firstly the correct working of the fluidic-based control of deformation was checked, the analysis performed confirmed that the serpentine loops are emptied orderly as to enhance a single channel deformation, moreover fluid ejection was complete allowing the membrane to slide into the etched channels. Afterwards the deformation achievable was tested staining the membrane prior to deformation, the imaging process to quantify deformation is still in progress, anyhow semi-quantitative analysis show a correlation between pressure and deformation, as the pressure is decreased on the glass-facing side of the membrane, the fluid is expelled from the etched channels and the membrane adheres to the channels contour thus being stretch. Preliminary data show a deformation of about 19%.

A final test with culture cells proved that it is possible to sterilize the culture chamber *via* ethanol wash and that cells can be seeded uniformly along the whole length of the channel thus laying the groundwork for further cells stretching experiments.

## BIBLIOGRAPHY


Ahmed W. W., T. Wolfram, A. M. Goldyn, K. Bruellhoff, B. A.Rioja, M. Möller, J. P. Spatz, T. A. Saif, J. Groll and R. Kemkemer, *Myoblast morphology and organization on biochemically micro-patterned hydrogel coatings under cyclic mechanical strain*, Biomaterials **31** (2010) 250-258.

Allen D. G., B. Zhang and N. P. Whitehead, *Stretch-induced membrane damage in muscle: comparison of wild-type and mdx mice*, Advances in Experimental Medicine and Biology, **682** (2010), 297-313.

Balachandran K., P. W. Alford, J. Wylie-Sears, J. A. Goss, A. Grosberg, J. Bischoff, E. Aikawa, R. A. Levine and K. K. Parker, *Cyclic strain induces dual-mode endothelialmesenchymal transformation of the cardiac valve*, PNAS, **108** (2011) 19943-19948.

Balestrini J. L., J. K. Skorinko, A. Hera, G. R. Gaudette and K. L. Billiar, *Applying controlled non-uniform deformation for in vitro studies of cell mechanobiology,* Biomech Model Machanobiol, **9** (2010) 329-344.

Curtis M. W. and B. Russell, *Micromechanical regulation in cardiac myocytes and fibroblasts: implications for tissue remodeling*, Eur J Physiol (2011), **462**, 105-117.

De Deyne P. G. *Formation of sarcomeres in developing myotubes: role of mechanical stretch and contractile activation*, Am J Physiol Cell Physiol (2000) **279**, C1801-C1811.

Dudley R. W. R., G. Danialou, K. Govindaraju, L. Lands, D. E. Eidelman and B. J. Petrof *Sarcolemmal Damage in Dystrophin Deficiency IsModulated by Synergistic Interactions betweenMechanical and Oxidative/Nitrosative Stresses*, Am J Pathol (2006), **168**:1276–1287

Fanchaouy M., E. Polankova, C. Jung, J. Ogrodnik, N. Shirokova and E. Niggli, *Pathways of abnormal stress-induced $Ca^{2+}$ influx into dystrophic mdx cardiomyocytes*, Cell Calcium, **46** (2009) 114-121.

Formigli L., E. Meacci, C. Sassoli, R. Squecco, D. Nosi, F. Chellini, F. Naro, F. Francini and A. Zecchi-Orlandini, *Cytoskeleton/Stretch-Activated Ion Channel InteractionRegulates MyogenicDifferentiation of SkeletalMyoblasts,* J. Cell. Physiol. (2007)**211**: 296–306.

Guan J., F. Wang, Z. Li, J. Chen, X. Guo, J. Liao and N. I. Moldovan, *The stimulation of the cardiac differentiation of mesenchymal stem cells in tissues constructs that mimic myocardium structure and biomechanics*, Biomaterials (2011), **32**, 5568-5580.

Hanke N., H. P. Kubis, R. J. Scheibe, M. Berthold-Losleben, O. Hüsing, J. D. Meissner and G. Gros, *Passive mechancal forces upregulate the fast myosin heavy chain IId/x via integrin and p38 MAP kinase activation in a primary muscle cell culture*, Am J Cell Physiol (2010), **298**, C910-C920

Iliescu C., F. E. H. Tay and J. Miao, *Strategies in deep wet etching of Pyrex glass,* Sensor and Actuators, **133** (2007) 395-400.

Kook S. H., H. J. Lee, W. T. Chung, I. H. Hwang, S. A. Lee, B. S. Kim and J. C. Lee *Cyclic mechanical stretch stimulates the proliferation of C2C12 myoblasts and ihibits their differentiation via prolonged activation of p38 MAPK*, Mol cells, **25** 479-486.

Kumar A., R. Murphy, P. Robinson, L. Wei and A. M. Boriek, *Cyclic mechanical strain inhibits skeletal myogenesis through activation of focal adhesion kinase, Rac-1 GTPase and NF-_B transcription factor*, The FASEB Journal, **18**, (2004).

Le Grand F. and M. A. Rudnicki, *Skeletal muscle satellite cells and adult myogenesis*, Current Opinion in Cell Biology, **19**, 628-633 (2007).

McCain M. L. and K. K. Parker, *Mechanotrasduction: the role of mechanical stress, myocyte shape, and cytoskeletal architecture on cardiac function*, Pflugers Arch- Eur J Physiol, **462** (2011) 89-104.

Meriane M., P. Roux, M. Primig, P. Fort andC. Gauthier-Rouvière*Critical Activities of Rac1 and Cdc42Hs in SkeletalMyogenesis: Antagonistic Effects of JNK and p38Pathways*, Molecular Biology of the Cell (2000) **11**, 2513–2528.

Michelin F., *Sviluppo di una piattaforma microfluidica per il controllo della concentrazione di ossigeno in culture cellulari*, Tesi di Laurea Magistrale in Ingegneria Chimica e dei Processi Industriali. 2009-2010.

Monk D. J., D. S. Soane and R. T. Howe, *A diffusion/chemical reaction model for HF etching of LPCVD phosphosilicate glass sacrificial layers*, IEE (1992).

Nakai N., F. Kawano, Y. Oke, S. Nomura, T. Ohira, R. Fujita and Y. Ohira *Mechanical stretch activates signaling events for protein translation initiation and elongation in C2C12 myoblasts*, Mol Cells (2010), **30**, 513-518.

Salameh A., A. Wustmann, S. Karl, K. Blanke, D. Apel, D. Rojas-Gomez, H. Franke, F. W. Mohr, J. Janousek and S. Dhein, *Cyclic mechanical stretch induces cardiomyocytes orientation and polarization of the gap junction protein connexin43*, Circ Res (2010), **106**, 1592-1602.

Tatsumi R., S. M. Sheehan, H. Iwasaki, A. Hattori and R. E. Allen *Mechanical stretch induces activation of skeletal muscle satellite cells in vitro*, Experimental Cell Research (2001), **267**, 107-114.

Tulloch N. L., V. Muskheli, M. V. Razumova, F. S. Korte, M. Regnier, K. D. Hauch, L. Pabon, H. Reinecke and C. E. Murry, *Growth of engineered human myocardium with mechanical loading and vascular coculture*, Circ Res. **109** (2011) 47-59.

Verma S. K., H. Lal, H. B. Golden, F. Gerilechaogetu, M. Smith, R. S. Guleria, D. M. Foster, G. Lu and D. E. Dostal, *Rac1 and RhoA differentially regulate angiotensinogen gene expression in stretched cardiac fibroblasts*, Cardiovascular Research, **90** (2011) 88-96.

Wan C., S. Chung and R. D. Kamm, *Differentiation of embryonic stem cells into cardiomyocites in a compliant microfluidic system*, Annals of Biomedical Engineering, **39** (2011) 1840-1847.

Yeung E. W. And D. G. Allen, *Stretch-activated channels in stretch-induced muscle damage: role in muscular dystrophy*, Clinical and Experimental Pharmacology and Physiology, **31** (2004) 551-556.

Yung Y. C., H. Vandenburgh and D. J. Mooney, *Cellular strain assessment tool (CSAT): precision-controlled cyclic uniaxial tensile loading*, J. of Biomechanics, **42** (2009) 178-182.

Suchyna T. M. and F. Sachs, *Mechanosensitive channel* properties and membrane mechanics in mouse dystrophic myotubes, *J Physiol,***581.1**, (2007) 369–387

Zhu H., M. Holl, T. Ray, S. Bhushan and D.R. Meldrum, *Characterization of deep wet etching of fused silica glass for sigle cell and optical sensor deposition,* J. Micromech. Microeng. **19** (2009) 065013

# Acknowledgments

I would like to deeply thank my supervisor Dr. Nicola Elvassore for his precious help, he was able to guide me through this work yet letting me develop my ideas, this approach really made me grow both as a person and as a researcher. All my gratitude goes also to the Bioera lab, Federica, Stefano, Enrico, Francesco, Alice, Sebastian, Giovanni, Camilla, Susi, Alessandro, Eleonora and Onelia for all the help they gave me when I needed it, it was great to work in such a close-knit group.

A special thanks goes to my beloved parents, Giovanni and Christina, they taught me to always give my best and always supported me, pushing me forward in the bad periods and rejocing with me in the good ones, I really couldn't ask for better parents. Also my sister Irene deserves a special mention, she was always there when I needed help, ready to cheer me up.
I would like to thank also my grandparents, Annamaria, Terenzio and (papou) Peter, and my aunt Lydia and uncle Kirk for their inconditionate love and support throughout this years.
A sincere thank also to my boyfriend Leonardo, he always enligthens my darkest day and was able to put up with me in this difficult period, I feel so lucky to have him in my life.

Finally I would like to thank all my friends, starting with Rachele and Mauro for their precious help looking for shoes and dresses for my graduation and the nice times spent together (I'll never forget "iotelia"), my classmates Riccardo, Matteo and Federico, I'll miss our card games, and Emilio always able to relax me with his calm, a big thank also to Giulia and Guido, even though we don't have time to catch up frequently lately its always nice to see each other and spend time together.
A deep thanking goes also to the legendary CUS group, Anna, Elia, Ale, Giorgia, Irene, and the new entries Silvia and Mattia, its great to have friends like you.

*Lía*